1972

Prediction of heated effluent dispersion in a stream using similitude techniques

Max Myron DeLong
Iowa State University

Prediction of heated effluent dispersion in a stream using similitude techniques

by

Max Myron DeLong

A Dissertation Submitted to the
Graduate Faculty in Partial Fulfillment of
The Requirements for the Degree of
DOCTOR OF PHILOSOPHY

Major Subject: Nuclear Engineering

Approved:

Signature was redacted for privacy.
In Charge of Major Work

Signature was redacted for privacy.
For the Major Department

Signature was redacted for privacy.
For the Graduate College

Iowa State University
Ames, Iowa

1972

TABLE OF CONTENTS

I. INTRODUCTION

Individuals, organizations and governments are becoming increasingly concerned about river water quality and the quality of the associated environment. This concern along with the existence of enforceable water quality standards is creating public and legal pressure on potential river water users to declare what effects might occur if the proposed use is allowed. When the proposed use involves diversion of part of the flow, addition of thermal energy to that portion and then returning it, estimates of the effects require prediction of the temperature patterns that result when the returned heated water mixes with the unused portion. Similitude techniques can be used to design a physical model of the heated discharge-river system, and data from this model can be used to predict temperature patterns in the prototype. However, the accuracy of the temperature predictions may be influenced by the engineering decisions required to achieve a model which is acceptable from a strictly hydraulic viewpoint. This study investigates the influence of the engineering decision of vertical dimension distortion on temperature prediction from model data.

A situation where there is concern about thermal energy additions to a water course exists when an electric power plant is to be sited near a river, and the river water is to be used in a once through manner as the primary coolant for the

steam condensors. The data in Table I indicate why this type of cooling, referred to as run of river cooling, is economically attractive.

Table I. Economic comparison of cooling methods

Heat Rejection Method	Cost [14][a] $/Kw (e)
Run of river cooling	5
Bay or lake cooling	6
Cooling pond	10
Mechanical draft cooling towers	
Wet	12
Dry	35
Natural draft cooling towers (hyperbolic)	
Wet	15
Dry	30

[a]Numbers in brackets refer to references listed at the end.

The potential impact of heated effluent (water) discharges from large nuclear or fossil fueled electric generating stations can be gauged by realizing that the temperature rise of the water may be 15-20°F and the required water quantity may be 10-20% of the average stream flow rate. Even though some proposed power stations may be so large as to preclude the use of run of river cooling, there will probably be smaller power plants and industrial plant sites where the problem of

temperature prediction may still be required to assess the potential effect of thermal energy additions on the stream biota, the stream's waste assimilative capacity, and on the subsequent use of the stream water.

There are two basic arrangements of discharging heated effluent into a cooler body of water. It may be discharged as a surface or subsurface layer or as a mixing jet. The latter case is defined by the situation where the effluent has considerably more velocity than the receiving waters. The layered discharge with a river as the receiving body results in much or all of the heated effluent being carried downstream from the discharge vicinity. The vertical and lateral mixing will depend primarily on the discharge structure design and the ambient turbulence of the river.

The type of discharge scheme investigated in this study is a layered discharge such as that resulting from a canal, conveying the heated effluent, and emptying into a river.

The common practice for modeling a heated effluent discharge-river system for temperature prediction is to build two models. One model is designed to achieve geometrical similarity of all three spatial dimensions, but it encompasses only the immediate vicinity around the heated effluent discharge structure. The second model is designed to encompass a much longer reach of the river. To achieve reasonable length and width dimensions in the second model, actual

dimensions must be reduced substantially; if the horizontal and vertical dimensions are reduced by the same fraction, flow depths of less than one quarter of an inch may result in the model. This small flow depth in the model presents hydraulic problems because surface tension forces in the model become prominent, and they are not prominent in the full scale situation. To eliminate this problem the vertical dimensions are reduced by a different ratio than the horizontal dimensions, and this practice is referred to as vertical scale distortion. For example, the horizontal dimensions in the prototype may be reduced so that 1000 length units in the prototype equal one unit in the model, but the vertical dimensions are reduced so that 100 length units in the prototype equal one unit in the model. The effects of vertical dimension distortion on heated effluent dispersion in the model are not well understood. It is usually assumed that the model with no vertical dimension distortion adequately represents the prototype temperature pattern in the vicinity of the discharge, and data from the first model is used to achieve proper spatial temperature patterns in the vicinity of the discharge in the second model. The second model is then used to determine a) if recirculation between discharge and intake occurs and b) an estimate of the temperature patterns downstream from the discharge.

However, the downstream temperature patterns predicted from the distorted model may not be accurate because of the vertical dimension distortion. This study investigates the effects of vertical dimension distortion on the dispersion of the heated effluent.

II. REVIEW OF LITERATURE

The current interest in the effects of thermal energy additions by man to the environment has resulted in symposia whose proceedings provide definitions, engineering solutions, economic aspects and unsolved facets of the problem.

The state-of-the-art of the engineering aspects of this subject is concisely discussed by Parker and Krenkel [14]. They have used in their discussion information presented at a symposium on the "Engineering Aspects of Thermal Pollution" [15], and they have provided a substantial number of references. Modeling of heated effluent dispersion is treated specifically in these references. It is stated that in addition to achieving flow pattern similarity in the receiving fluid attention should be given to the possible restrictions on the choice of remaining model variables resulting from various stages of heated effluent dispersion that are pertinent to a particular situation. Those stages of dispersion that pertain to the layered discharge being studied here are a) mass transport of the effluent by ambient currents and b) dispersion due to turbulence in the ambient fluid. The opinion is given in reference [14] that similarity of ambient turbulence cannot be achieved in a model with vertical dimension distortion.

Frazer et al. [9] in interpreting work by Barr [2] concludes that sufficient dispersion in a model of a well mixed estuary, namely little vertical variation of salinity, is

achieved by properly simulating the tide depth profile. Proper simulation of depth profiles is just a statement of geometrical similarity but achieving proper similarity may not be straight forward according to Frazer et al. [9]. Barr [1] suggests that a guide to the required roughness in the various reaches of the model estuary can be obtained from a Stanton type resistance diagram for open channel flow.

Several references [1, 2, 3, 10, 15, 16] propose and attempt to justify various design criteria for modeling heated discharges, but the approach presented by Murphy [12] for modeling any system is the most systematic.

Since much of the equipment built and described by Bull [4] was utilized in this study guidelines for establishing operating velocities, flow rates and temperatures were taken from reference [4]. The desired surface temperature patterns were based on those reported by Merriman [11] for a situation where heated effluent from an operating nuclear powered electric generating station was discharged into a river.

Theoretical studies related to this problem but not directly applicable have been done by Edinger and Polk [6] and by Elder [7]. In reference [6] a heated effluent discharge-river situation is investigated analytically, but the river is assumed to be of uniform velocity. In reference [7] coefficients of dispersion for an injection of dye were derived for shear flow in a wide channel and were compared with experimental results. The coefficients apply to the entire channel

cross-section and thus contain no vertical dimension dependency.

Basic references on fluid mechanics [18], open channel flow [5], turbulence [8] were used for defining parameters.

III. ANALYTICAL RELATIONSHIPS

The design of a hydraulic model can be done in a very systematic way by following the procedure presented by Murphy [12]. First, the variable to be studied and the variables that are assumed to influence it are listed. The variables for this study are listed in Table II. It has been assumed that the mixing of the heated effluent with the ambient fluid is dominated by turbulent dispersion. The model will be operated in a steady state condition. The cross section of the main channel will be constant and trapezoidal, and the cross section of the effluent channel will be constant and rectangular. The flow depth will be constant. The volume flow rate of the heated effluent is to be 15% of the combined flow rates.

The general functional relation for the temperature is

$$\Delta t = f(\Delta t_o, V_o, V, \ell, B, D, C, S, W, E, x', y', z', \lambda, \rho, \mu, g, \phi, r) \qquad (1)$$

Table II indicates that 20 variables expressed in four dimensions are used to describe the functional relation. Using the Buckingham Pi Theorem the number of dimensionless groups, or Pi terms, is determined by the difference between the number of variables and the number of dimensions used to express them; namely 20 - 4 = 16 Pi terms. The Pi terms may also be used to describe the phenomenon.

Table II. Significant variables

Symbol			Dimensions[a]
1.	Δt	Temperature difference between any point and a reference temperature	θ
2.	Δt_o	Temperature difference between heated effluent and ambient stream temperature	θ
3.	V_o	Velocity of effluent	LT^{-1}
4.	V	Velocity at any other point	LT^{-1}
5.	ℓ	Reference length	L
6.	B	Main channel bottom width	L
7.	D	Main channel flow depth	L
8.	C	Slope of sides of main channel	-
9.	S	Main channel bottom slope in downstream direction	-
10.	W	Effluent channel width	L
11.	E	Effluent channel depth	L
12.	x'	Downstream distance from coordinate origin where Δt is measured	L
13.	y'	Vertical distance from coordinate origin where Δt is measured	L
14.	z'	Lateral distance from coordinate origin where Δt is measured	L
15.	λ	Any significant length	L
16.	ρ	Density of the fluid	ML^{-3}
17.	μ	Viscosity of the fluid	$ML^{-1}T^{-1}$
18.	g	Acceleration of gravity	LT^{-2}
19.	ϕ	Relative humidity of air	--
20.	r	Relative roughness	--

[a] L = length, M = mass, T = time and θ = temperature difference.

One possible set is

$$\frac{\Delta t}{t_o} = f_1\left(\frac{V}{V_o}, \frac{B}{\ell}, \frac{D}{\ell}, S, \frac{W}{\ell}, \frac{E}{\ell}, C, \frac{x'}{B}, \frac{y'}{B}, \frac{z'}{B}, \frac{\lambda}{\ell}, \frac{V^2}{g\lambda}, \right.$$

$$\left. \frac{\rho V\lambda}{\mu}, \phi, r\right) \tag{2}$$

Equation (2) is entirely general and it applies to any other system which is a function of the same variables. Therefore a second functional expression for a model could be written as

$$\frac{\Delta t_m}{\Delta t_{om}} = f_{1m}\left(\frac{V_m}{V_{om}}, \frac{B_m}{\ell_m}, \frac{D_m}{\ell_m}, S_m, \frac{W_m}{\ell_m}, \frac{E_m}{\ell_m}, C_m, \frac{x'_m}{B_m}, \frac{y'_m}{B_m}, \right.$$

$$\left. \frac{z'_m}{B_m}, \frac{\lambda_m}{\ell_m}, \frac{V_m^2}{g_m\lambda_m}, \frac{\rho_m V_m \lambda_m}{\mu_m}, \phi, r\right) \tag{3}$$

Throughout this discussion the variables with an 'm' subscript refer to the model and those variables with no subscript refer to the prototype.

Since the same phenomenon is involved in both the prototype and the model, the function f_{1m} must be identical with the function f_1, and if each term on the right hand side of Equation (2) is made equal to the corresponding term on the right hand of Equation (3), then

$$\frac{\Delta t}{\Delta t_o} = \frac{\Delta t_m}{\Delta t_{om}} \tag{4}$$

Equation (4) is called the prediction equation because it may be used to predict the temperature Δt of the prototype from the measured temperature Δt_m in the model.

The design conditions for the model are established by equating the corresponding terms of Equations (2) and (3). The design conditions are:

$$\frac{V_m}{V_{om}} = \frac{V}{V_o} \tag{5}$$

$$\frac{B_m}{\ell_m} = \frac{D}{\ell} \tag{6}$$

$$\frac{D_m}{\ell_m} = \frac{D}{\ell} \tag{7}$$

$$S_m = S \tag{8}$$

$$\frac{W_m}{\ell_m} = \frac{W}{\ell} \tag{9}$$

$$\frac{E_m}{\ell_m} = \frac{E}{\ell} \tag{10}$$

$$C_m = C \tag{11}$$

$$\frac{x'_m}{B_m} = \frac{x'}{B} \tag{12}$$

$$\frac{y'_m}{B_m} = \frac{x'}{B} \tag{13}$$

$$\frac{z'_m}{B_m} = \frac{z'}{B_m} \tag{14}$$

$$\frac{\lambda_m}{\ell_m} = \frac{\lambda}{\ell} \tag{15}$$

$$\frac{V_m^2}{g_m \lambda_m} = \frac{V^2}{g\lambda} \tag{16}$$

$$\frac{\rho_m V_m \lambda_m}{\mu_m} = \frac{\rho V \lambda}{\mu} \tag{17}$$

$$\phi_m = \phi \tag{18}$$

$$r_m = r \tag{19}$$

A length scale can be defined as

$$n = \frac{\ell}{\ell_m} \tag{20}$$

and normally $n > 1$ because the reason for building hydraulic models is usually to achieve a model of physically smaller dimensions than the prototype. However, in a laboratory where several channels are available the possibility exists for $n < 1$.

If the same fluid is used in the model and prototype

$$\rho_m = \rho \tag{21}$$

$$\mu_m = \mu \tag{22}$$

and, since both model and prototype will be operated under the same gravitational influence

$$g_m = g \tag{23}$$

Nondimensional distances will be defined as

$$x = \frac{x'}{B} \tag{24}$$

$$y = \frac{y'}{B} \tag{25}$$

$$z = \frac{z'}{B} \tag{26}$$

Using the constraints resulting from Equations (20), (21), (22) and (23) and the definitions from Equations (24), (25) and (26), Equations (6), (7), (9), (10), (12), (13), (14), (15), (16) and (17) can be rewritten as

$$B_m = \frac{B}{n} \tag{6a}$$

$$D_m = \frac{D}{n} \tag{7a}$$

$$W_m = \frac{W}{n} \tag{9a}$$

$$E_m = \frac{E}{n} \tag{10a}$$

$$x_m = x \tag{12a}$$

$$y_m = y \tag{13a}$$

$$z_m = z \tag{14a}$$

$$\lambda_m = \frac{\lambda}{n} \tag{15a}$$

$$V_m = \frac{V}{n^{1/2}} \tag{16a}$$

$$V_m = Vn \tag{17a}$$

Equations (6a), (7a), (9a), (10a), (12a), (13a), (14a) and (15a), are statements of the geometric similarity that are imposed on the model once a value for n has been selected. Equation (16) is a statement of the Froude number equality, and this criterion will be applied for defining model velocities. This leads to the mean flow velocities being related as in Equation (16a). Equation (17) is a statement of Reynolds Number equality. Equation (17a) indicates a contradiction compared to Equation (16a) in defining velocity relationships when the same fluid is used in both model and prototype. By definition [12], a model is "distorted" when one or more of the design conditions cannot be met, and therefore Equation (17a) leads to the conclusion that the model is distorted. This distortion will be neglected in this study.

Equation (18) states that the relative humidity should be the same in both model and prototype. This has been included in recognition of that fact that heat could be transferred from the stream to the air above it. However, it will be assumed that heat transfer from the channel to the air above is negligible.

A time scale between model and prototype is established from equating the gravitational constants. Dimensionally g has units of LT^{-2} and if time is designated by , then

$$\frac{g}{g_m} = 1 = \frac{\ell T^{-2}}{\ell_m T_m^{-2}} \tag{27}$$

and

$$\frac{T}{T_m} = n^{1/2} \tag{28}$$

The discharge for model and prototype systems can be obtained from the continuity equation,

$$Q = VA \tag{29}$$

where V = mean flow velocity

A = cross-sectional flow area

The discharge prediction equation is

$$\frac{Q}{Q_m} = \frac{VA}{V_m A_m} \tag{30}$$

and since $V = n^{1/2} V_m$ and $A/A_m = n^2$

$$\frac{Q}{Q_m} = n^{5/2} \tag{31}$$

Vertical dimension distortion can be defined by introducing distortion factors into the design condition equations which involve vertical dimensions. Thus

$$D_m = \frac{\alpha}{n} D \tag{32}$$

$$E_m = \frac{\alpha}{n} E \tag{33}$$

$$S_m = \beta S \tag{34}$$

$$C_m = \xi C \tag{35}$$

$$y_m = \alpha y \tag{36}$$

where

α = depth distortion factor

β = channel bottom slope distortion factor

ξ = channel side slope distortion factor

When a model has correctly distorted vertical dimensions $\beta = \xi = \alpha$.

For this study the characteristic length in Equation (16) has been chosen as the hydraulic depth. Thus, the Froude Number equality that is used to define the main channel velocity in the model becomes

$$\frac{V_m}{(g_m H_m)^{1/2}} = \frac{V}{(gH)^{1/2}} \tag{37}$$

where

$$\text{Froude No.} = Fr = \frac{V}{(gH)^{1/2}} \tag{38}$$

and

$$H = \text{hydraulic depth, ft.} = \frac{\text{flow area, ft.}^2}{\text{top width, ft.}}$$

Since the main channel cross section is trapezoidal,

$$H = \frac{(B + D/C)D}{(B + 2D/C)} \tag{39}$$

and

$$\frac{H_m}{H} = \frac{\alpha}{n} \frac{(B + 2D/C)(B + \alpha D/\xi C)}{(B + D/C)(B + 2\alpha D/\xi C)} \tag{40}$$

When $\xi = \alpha = 1$

$$\frac{H_m}{H} = \frac{1}{n} \tag{40a}$$

Reynolds Number distortion has been neglected, but Reynolds Number can still be used as a guide to evaluate whether or not the main channel model velocity is large enough to insure that viscous forces are not prominent in the model.

For this study

$$Re = \frac{\rho V R}{\mu} \tag{41}$$

where $R = \text{hydraulic radius} = \dfrac{\text{flow area, ft.}^2}{\text{wetted perimeter, ft.}}$

By keeping Re > 1400 viscous forces will not be prominent in open channel flow [5].

Since the main channel is trapezoidal

$$R = \frac{(B + D/C)D}{(B + (D/C)(1 + (1/C)^2)^{1/2}} \tag{42}$$

$$\frac{R_m}{R} = \frac{\alpha}{n} \frac{(B + \alpha D/\xi C) \quad (B + (D/C)(1 + (1/C)^2)^{1/2})}{(B + (\alpha D/\xi C)(1 + (1/\xi C)^2)^{1/2})(B + D/C)} \tag{43}$$

and for $\alpha = \xi = 1$

$$\frac{R_m}{R} = \frac{1}{n} \tag{44}$$

Chow [5] has stated that the Darcy-Weisbach head loss formula can be applied to uniform flows (constant depth) in open channels when written in the form

$$Se = f \frac{V^2}{8gR} \tag{45}$$

where Se = energy gradient = $\frac{\text{head loss, ft.}}{\text{distance, ft.}}$

f = friction factor

From Equation (45)

$$f = \frac{8gRSe}{V^2} \tag{46}$$

For $\alpha = 1$ and for correctly modeled surface roughness, $S_m = S$ and hence $Se_m = Se$. Since $R_m/R = 1/n$ and $V^2/V_m^2 = n$,

the friction factor ratio is

$$\frac{f_m}{f} = \frac{8gR_mSe_m}{V_m^2} \quad \frac{V^2}{8gRSe} = 1 \tag{47}$$

Murphy [12] states that if the prototype is relatively smooth it may not be possible to make the model sufficiently smooth to have $S_m = S$; and it may be necessary to distort the channel slope. If $S_m \neq S$, and hence $Se_m \neq Se$, then for $\alpha = 1$

$$\frac{f_m}{f} \neq 1 \tag{48}$$

For cases where depth distortion occurs in the model distortion of roughness, velocity and hydraulic radius will cause distortion of the friction factor. The friction factor has not been used as a Pi term in this development. However, knowledge of the magnitude of the ratio given in Equation (47) and of the distortion of velocities and hydraulic radii for a given experimental situation can provide information on the surface roughness distortion.

Distortion of the design conditions will have the effect of altering the prediction equation, Equation (4), to

$$\frac{\Delta t}{\Delta t_o} = \delta \frac{\Delta t_m}{\Delta t_{om}} \tag{4a}$$

where δ is a prediction factor. The prediction factor may be a function of the distortion factors, the Pi terms and the

length scale n.

Where $\Delta t_o = \Delta t_{om}$ the prediction factor becomes

$$\delta = \frac{\Delta t}{\Delta t_m} \tag{49}$$

The prediction factor may be a function of the Pi terms, distortion factors and possibly the length scale n.

$$\delta = f(\alpha,\beta,\xi,\ldots n, \frac{V}{V_o}, \frac{B}{\ell}, \frac{D}{\ell}, S, \frac{W}{\ell}, \frac{E}{\ell}, C, \frac{\lambda}{\ell}, \frac{V^2}{g\lambda},$$

$$\frac{\rho V\lambda}{\mu}, \phi, r) \tag{50}$$

However, if δ is to be determined from analysis of experimental data it may be expedient to hold constant many of the Pi terms and distortion factors in Equation (49). If it is assumed that the prediction factor is a function of only two variables while other variables are held constant it may be possible to form and validate an equation for

$$\delta = f(\alpha, \beta) \tag{51}$$

Procedures for developing functions such as Equation (51) where the variables may be combined by multiplication or addition are described by Murphy [12].

IV. EXPERIMENTAL APPARATUS

The experimental apparatus was a set of three main open channels each having a smaller open channel attached to it for discharging heated effluent into the mainstream. The three main open channels were built and used by Bull [4]. They had relative width and length dimensions of 4, 2 and 1. The mainstream channels had a trapezoidal cross section shape and the smaller heated effluent channels had a rectangular cross-section shape. A plan view of the channel system and the channel cross-section shapes are shown in Figure 1. The coordinate system is defined as shown in Figure 2. The channel designations and dimensions of the three systems are listed in Table III.

A schematic of the flow system is shown in Figure 3. The reservoir for the mainstream flow was a group of three interconnected stock tanks with the bottoms elevated approximately 7 feet from the laboratory floor. One of two pipes was used to transfer the flow to a mainstream channel forebay. The 1 1/4 inch diameter line had two valves, one to open and close the line and one to control the flow, and it was used with Channels 4 and 2. The 3 inch diameter line is used with Channel 8 and it had just one valve. Both the 1 1/4 inch and 3 inch lines were allowed to terminate above the surface of the water in the forebay.

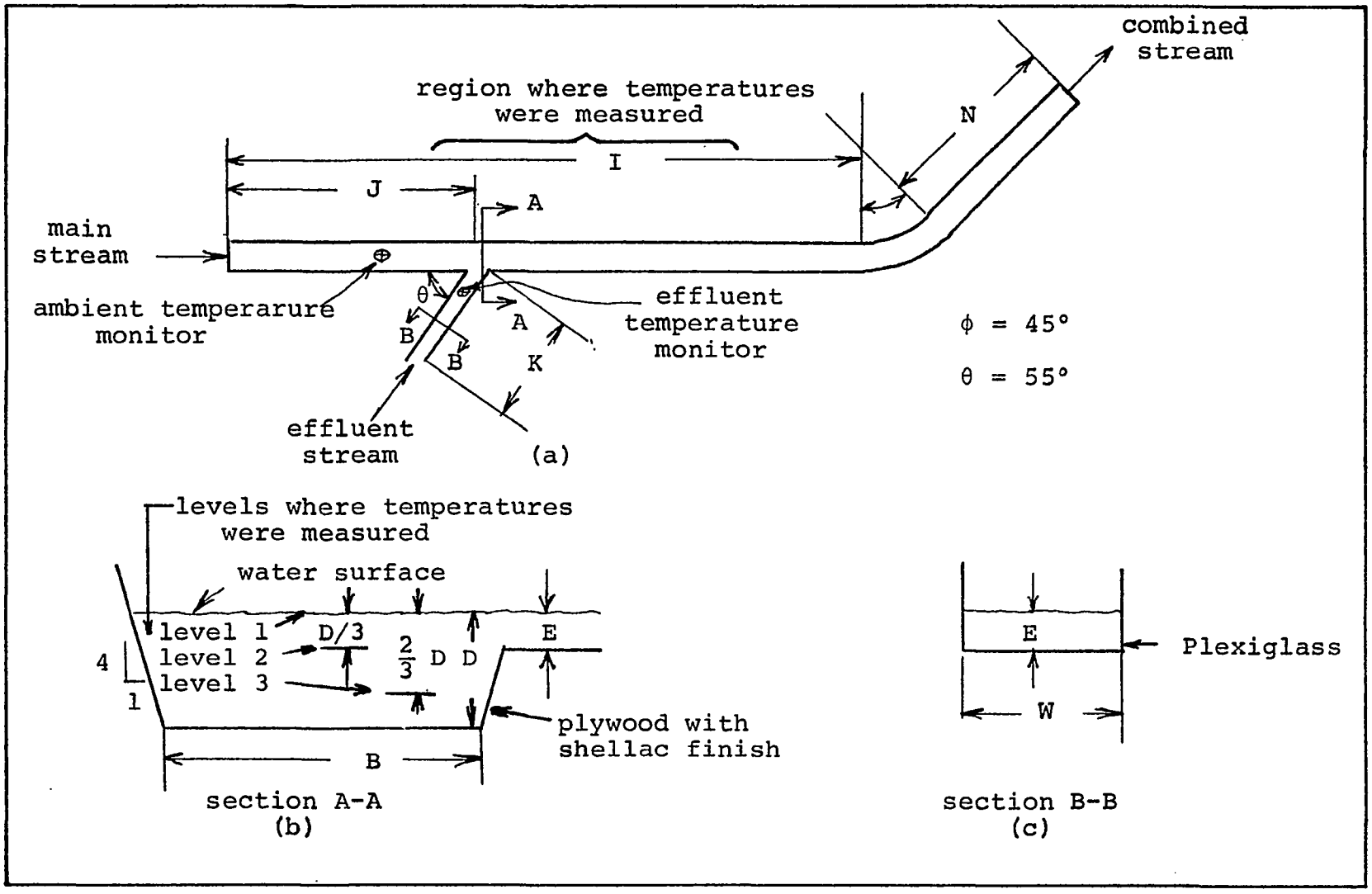

Figure 1. Channel system a) plan view; b) main channel cross section; c) effluent channel cross section. Actual dimensions in Table II

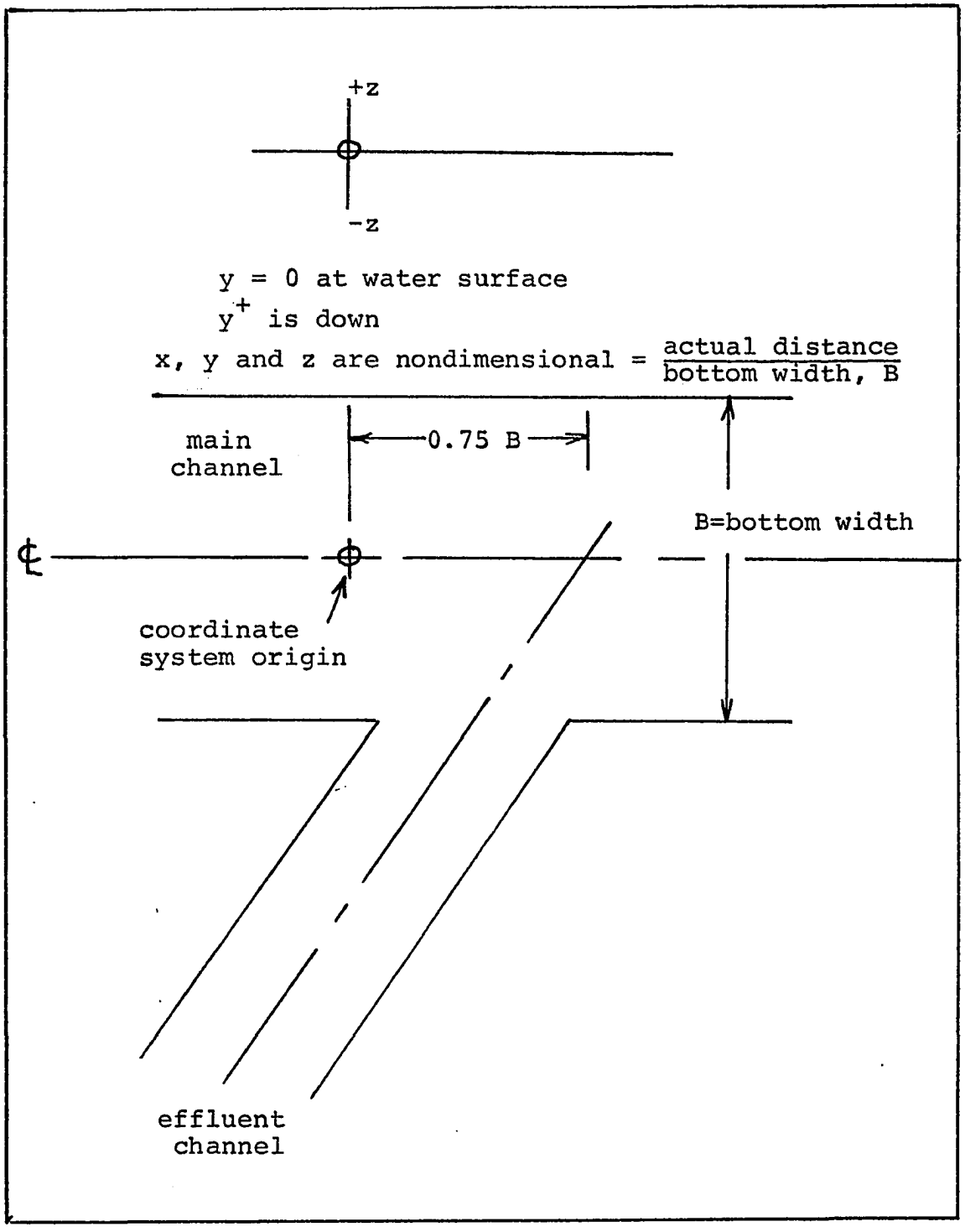

Figure 2. The coordinate system

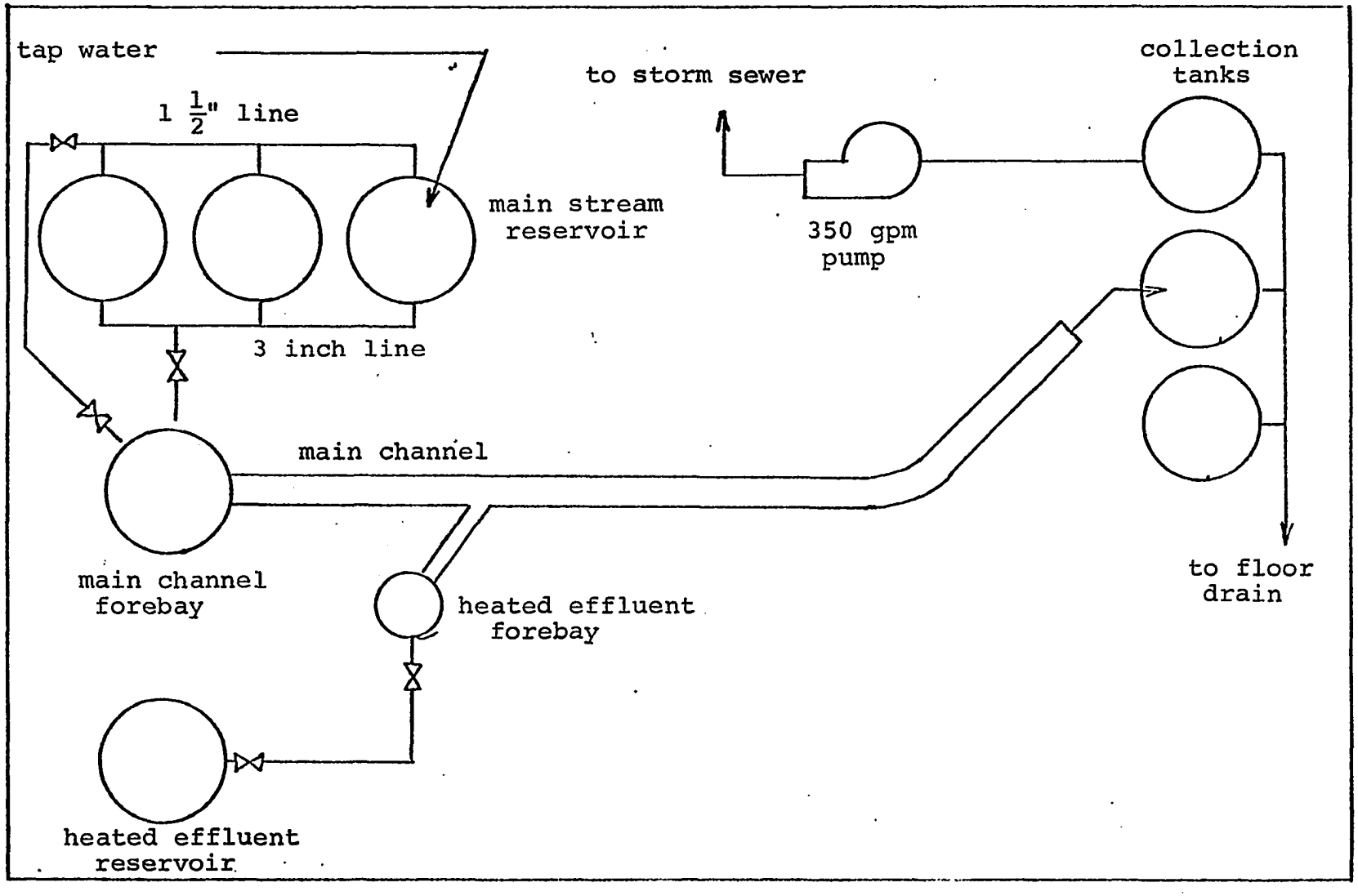

Figure 3. Flow system schematic

Table III. Channel designations and dimensions

Channel designation[a]	Dimensions shown in Figure 1							
	B (in.)	D (in.)	W (in.)	E (in.)	I (ft.)	J (ft.)	K (ft.)	N (ft.)
C8D3.0	8.00	3.00	4.00	1.00	20.0	8.0	1.5	6.0
C4D1.5	4.00	1.50	2.00	0.50	10.0	4.0	1.5	3.0
C4D2.25	4.00	2.25	2.00	0.75	10.0	4.0	1.5	3.0
C4D3.0	4.00	3.00	2.00	1.00	10.0	4.0	1.5	3.0
C2D0.75	2.00	0.75	1.00	0.25	5.0	2.0	1.5	1.5
C2D1.13	2.00	1.13	1.00	0.38	5.0	2.0	1.5	1.5
C2D1.5	2.00	1.50	1.00	0.50	5.0	2.0	1.5	1.5

[a]Channels 4 refers to the group C4D1.5, C4D2.25 and C4D3.0. Channels 2 refers to the group C2D0.75, C2D1.13 and C2D1.5.

Tap water at approximately 60°F and from a one inch line was used to maintain a constant level in the mainstream reservoir during the operation of a channel, and thus a constant flow rate was maintained. All water entering the forebay emptied into the mainstream channel.

The heated effluent reservoir was a 135 gallon stock tank located on the second floor of the laboratory building. The heated effluent was prepared by the batch since a continuous supply of make up water at the proper temperature and flowrate was not available. Variation in flowrate of the heated

effluent was minimized by the second story location of the tank. The elevation difference of 17 feet ± 1 foot between the tank water level and the models resulted in flow rate variations of less than 5%.

The water in the heated effluent reservoir was raised to the desired temperature, approximately 80°F, by filling the tank with cold tap water and heating it with a 4500 watt Chromalox immersion heater element or, the tank was filled with a mixture of hot and cold tap water. A two inch diameter line carried the heated effluent to the laboratory. The line was opened and closed by a valve at the reservoir and the flow rate was controlled by a valve near the heated effluent forebay.

Information for flow rate computation was obtained by diverting the main stream, heated effluent stream, or combined stream into a container on a platform scale, and noting the time required to obtain 50, 100, or 200 pounds of water.

The discharge from Channels 4 and 2 was collected in three interconnected stock tanks and then discharged to the floor drain. The floor drain did not have sufficient capacity to take all the discharge from Channel 8 so part of the discharge was pumped outside the laboratory building to the storm sewer.

Temperatures were measured with Yellow Springs Instrument Company Model 427 thermistors and a Model 425 F readout device. A switch box facilitated reading the temperatures at various

locations. The measured temperatures included a) those of the combined stream in the region of the channel being studied; b) the main stream or ambient temperature at a position of approximately 0.5-1.0 feet upstream from the discharge of heated effluent; c) the heated effluent temperature at a position of approximately 10 inches before the effluent merged with the main stream; and d) the heated effluent reservoir temperature. The locations of the temperature measurements are shown in Figure 1.

The thermistors were a button type with a flexible lead. The leads were taped to steel rods. The thermistors used to measure the channel temperatures were mounted in a fixture similar to the sketch in Figure 4. The number of thermistors mounted in the fixture ranged from 5-9 depending on the channel being examined. At a fixed x and y position a set of temperatures could be measured along the z axis.

The thermistor time constant has been measured by another investigator [17] and found to be .7 seconds.

A twelve inch machinists level placed on top of a 4 foot long carpenters level was used in determining the channel bottom slope. One end of the carpenters level was raised until the vial of the machinists level indicated a level condition. The elevation difference between the two ends of the carpenters level was noted and the slope computed.

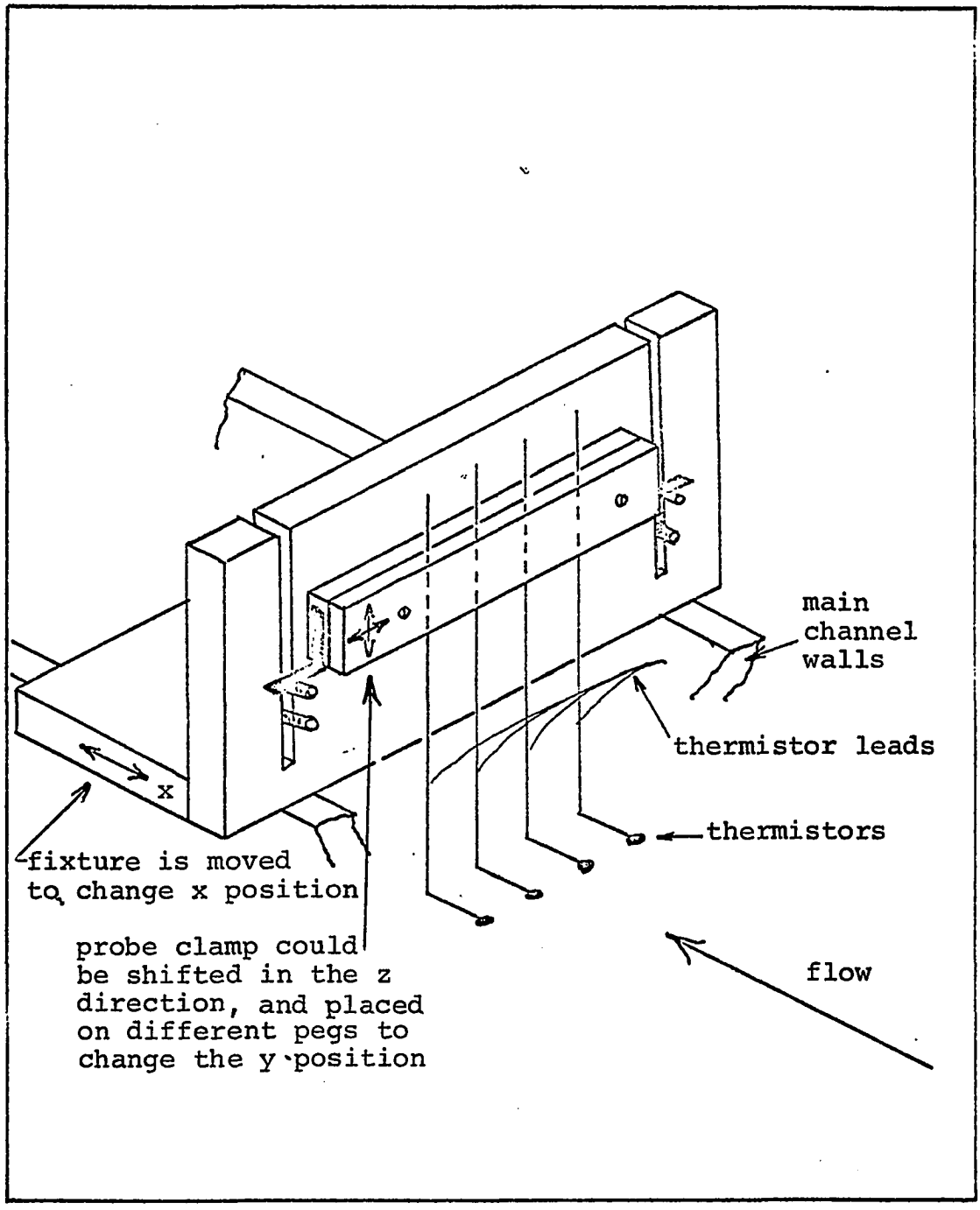

Figure 4. Thermistor mounting fixture

V. EXPERIMENTAL PROCEDURE

Preliminary tests were conducted with Channels 4 to determine the general character and temperature of the warm water plume. The main stream flow rates that were used were nearly the same as those used by Bull [4]. A combined stream mean velocity of 0.65 ft/sec., a flow depth of 1.5 inches, a ratio of effluent flow rate to combined flow rate of 15% and an initial temperature difference of 20°F were used at first. However, with those conditions the surface isotherms in the vicinity of the effluent discharge were a maximum of only 10-12°F above the main stream ambient temperature, and there was considerable surface irregularity at the point where the two streams joined. These conditions were apparently causing rapid mixing and did not result in surface isotherms near the initial effluent temperature as described by Merriman [11]. The mean velocity of the combined stream was then reduced to approximately 0.54 ft/sec.. With the same depth and flow rate ratios as used initially, isotherms in the range of 16-20°F were produced in the vicinity of the discharge; and other isotherms could be identified with the temperature measuring equipment up to distances of 6-10 stream widths downstream. These were the desired characteristics of the plume. Appropriate dimensions and velocities for the other channels were based on the design equations and the constraints of the dimensions of the existing channels. The parameters for the

other channels were determined using a computer program.

From the seven different tests described in Table IV, thirty model-prototype combinations were used. The various combinations are listed in Table V.

Preparation for a test began by attaching the effluent channel to the main channel and attaching forebays to both channels. The seams of the main channel were caulked where required. The control valve for the main channel flow was adjusted until the proper flow rate was obtained. Flow rate was measured using the platform scale and noting the time required to accumulate a certain weight of water.

The channel bottom slope and the weir at the end of the channel were adjusted to achieve a uniform flow condition, namely constant depth, for a distance of approximately 3 channel widths upstream and approximately 15 channel widths downstream from the intersection of the effluent and main streams. The depth of flow in the main channel was set at approximately 85% of the required combined stream depth. Then the heated effluent was allowed to flow, and its flow rate was established either by measuring just it or by measuring the combined stream flow rate. With the heated effluent added to the main channel flow, the depth was again checked to determine if the proper combined stream depth and uniform flow conditions in the region to be examined were being achieved.

Table IV. Experimental parameters

Parameter	Channel designation						
	C8D3.0	C4D1.5	C4D2.25	C4D3.0	C2D0.75	C2D1.13	C2D1.5
Combined stream depth, ft.	0.250	0.125	0.188	0.250	0.063	0.093	0.125
Combined stream mean velocity, fps	0.77	0.53	0.65	0.74	0.38	0.46	0.52
Combined stream flow rate, cfs	0.1395	0.0247	0.0464	0.0733	0.0043	0.0082	0.0130
Combined stream Froude No.	0.281	0.281	0.281	0.281	0.281	0.281	0.281
Combined stream Reynolds No.[a]	10,115	3576	5530	7405	1264	1955	2618
Channel bottom slope	0.00195	0.00260	0.00260	0.00260	0.00195	0.00195	0.0026
Effluent to combined flow flow rate ratio,%	15	15	15	15	15	15	15
Effluent stream depth, ft.	0.083	0.042	0.062	.083	0.021	0.031	0.042
Effluent stream mean velocity, fps	0.753	0.53	0.67	0.79	0.38	0.47	0.56
Effluent stream flow rate, cfs	0.0209	0.0037	0.0070	0.0110	0.0006	0.0012	0.0019
Effluent stream Froude No.	0.460	0.46	0.48	0.49	0.46	0.48	0.50
Effluent stream Reynolds No.[a]	3586	1268	2047	2828	448	723	999

[a]Kinematic viscosity = 1.168×10^{-5} ft^2/sec [18].

Table IV (Continued)

Parameter	Channel designation						
	C8D3.0	C4D1.5	C4D2.25	C4D3.0	C2D0.75	C2D1.13	C2D1.5
Combined stream hydraulic radius, ft.	0.154	0.077	0.099	0.117	0.038	0.0495	0.0583
Combined stream flow area, $ft.^2$	0.182	0.046	0.071	0.099	0.0114	0.0178	0.0247
Combined stream hydraulic depth, ft.	0.230	0.1151	0.1669	0.2159	0.0576	0.0835	0.108
Effluent stream hydraulic radius, ft.	0.0555	0.0277	0.357	0.0417	0.0139	0.0179	0.0208
Effluent stream flow area, $ft.^2$	0.0277	0.0069	0.0104	0.0139	0.0017	0.0026	0.0035

Table V. Prototype - model combinations

	Prototype[a]	Model[a]	n	α
1.	C8D3.0	C4D1.5	2	1.00
2.	C8D3.0	C4D2.25	2	1.50
3.	C8D3.0	C4D3.0	2	2.00
4.	C8D3.0	C2D0.75	4	1.00
5.	C8D3.0	C2D1.13	4	1.50
6.	C8D3.0	C2D1.5	4	2.00
7.	C4D1.5	C2D0.75	2	1.00
8.	C4D1.5	C2D1.13	2	1.50
9.	C4D1.5	C2D1.5	2	2.00
10.	C4D2.25	C2D0.75	2	0.67
11.	C4D2.25	C2D1.13	2	1.0
12.	C4D2.25	C2D1.5	2	1.33
13.	C4D3.0	C2D0.75	2	0.50
14.	C4D3.0	C2D1.13	2	0.75
15.	C4D3.0	C2D1.5	2	1.00

[a]Each pair above can be reversed and another 15 combinations with reciprocal values of n and α will result.

Once the required flow rates and depths were achieved temperature measurements were taken. Because of the random nature of stream turbulence, and hence mixing, temperature readings for a particular thermistor at a particular location varied with time. The indicated variation ranged from less than $\pm$ 1/2 to $\pm$ 4°F. To obtain an average temperature the readout device was observed for 5-10 seconds, and a temperature representing the average needle position was recorded.

The usual order of taking temperature measurements was to start at level 1, the surface, and at x = 0. The coordinate system is defined in Figure 2. A set of temperatures along the z axis was obtained along with the ambient main stream and initial effluent temperatures. Then for Channels 4 and C8D3.0 the thermistor probe was shifted along the z axis a distance equal to one-half the thermistor spacing, and another set of temperatures was obtained along with the ambient main stream and initial effluent temperatures. This shifting of the probe clamp achieved a finer spatial grid.

The fixture was moved to new x positions in increments of $\Delta x = 0.125$ in the vicinity of the discharge, and $\Delta x = 0.25$ farther downstream, until $x \simeq 6$ was reached. This would constitute one run. A run was repeated at least three times for level 1 measurements, and a fourth run was done if there were many deviations of 4-6°F in the recorded data. For levels 2 and 3 the variation of indicated temperature was much less.

At least two runs were obtained for each channel and a third run was obtained if many large deviations occurred.

VI. RESULTS AND DISCUSSION

A. Preliminary Data Analysis

Temperature readings for a particular coordinate position in the channel required conversion to temperature differences, normalizing and averaging before they could be used in the data analysis. The temperature difference was obtained by subtracting the ambient temperature of the main stream from the measured temperature. The normalizing was done to compensate for the variations of the desired 20°F initial temperature difference between the effluent stream and the main stream. Variations resulted from changes in tap water temperature during a run. The tap water was used as makeup for the main stream reservoir. The variation of the initial temperature difference was a maximum of $\pm$ 2°F. The normalized temperature differences were computed using Equation (32)

$$\Delta t'_{normalized} = (\Delta t_{measured}) \left[\frac{\text{Desired initial temperature difference, } \Delta t'_o}{\text{measured initial temperature difference, } \Delta t_o} \right] \quad (52)$$

The normalized temperature differences for each coordinate position were averaged and rounded off to the nearest whole number. The normalized and averaged data for the various channels are tabulated in the Appendix.

A brief qualitative description of the surface $\Delta t'$ isotherm positions with and without design condition distortions will be presented as an introduction to the qualitative analysis of the data. The surface $\Delta t'$ isotherms for the prototype-model combination C8D3.0 and C2D0.75, where $n = 4$ and $\alpha = 1$, are shown in Figures 5a and b. The various isotherms in Figures 5a and b extend downstream approximately the same distance and appear to be similarly oriented.

The surface isotherms for the combination C8D3.0 and C4D1.5, where $n = 2$ and $\alpha = 1$, are shown in Figures 6a and b. For this combination the model channel bottom slope is 133% of that dictated by design conditions. The surface isotherms for C4D1.5 are oriented similarly but corresponding isotherms are generally shifted upstream.

The surface isotherms for the combination C8D3.0 and C4D3.0, where $n = 2$ and $\alpha = 2$, are shown in Figures 7a and b. For this combination the model channel slope is 67% of that dictated by model design conditions. The surface isotherms for C4D3.0 are closer to the channel side wall than in the prototype, and corresponding isotherms are shifted downstream from those in the prototype. For two of the combinations discussed in the preceding paragraphs, one or more design conditions were distorted. A rigorous procedure is required to determine if the prediction factor, $\delta = \frac{\Delta t'}{\Delta t'_m}$, can be expressed as a function of the distortion factors and the length scale n.

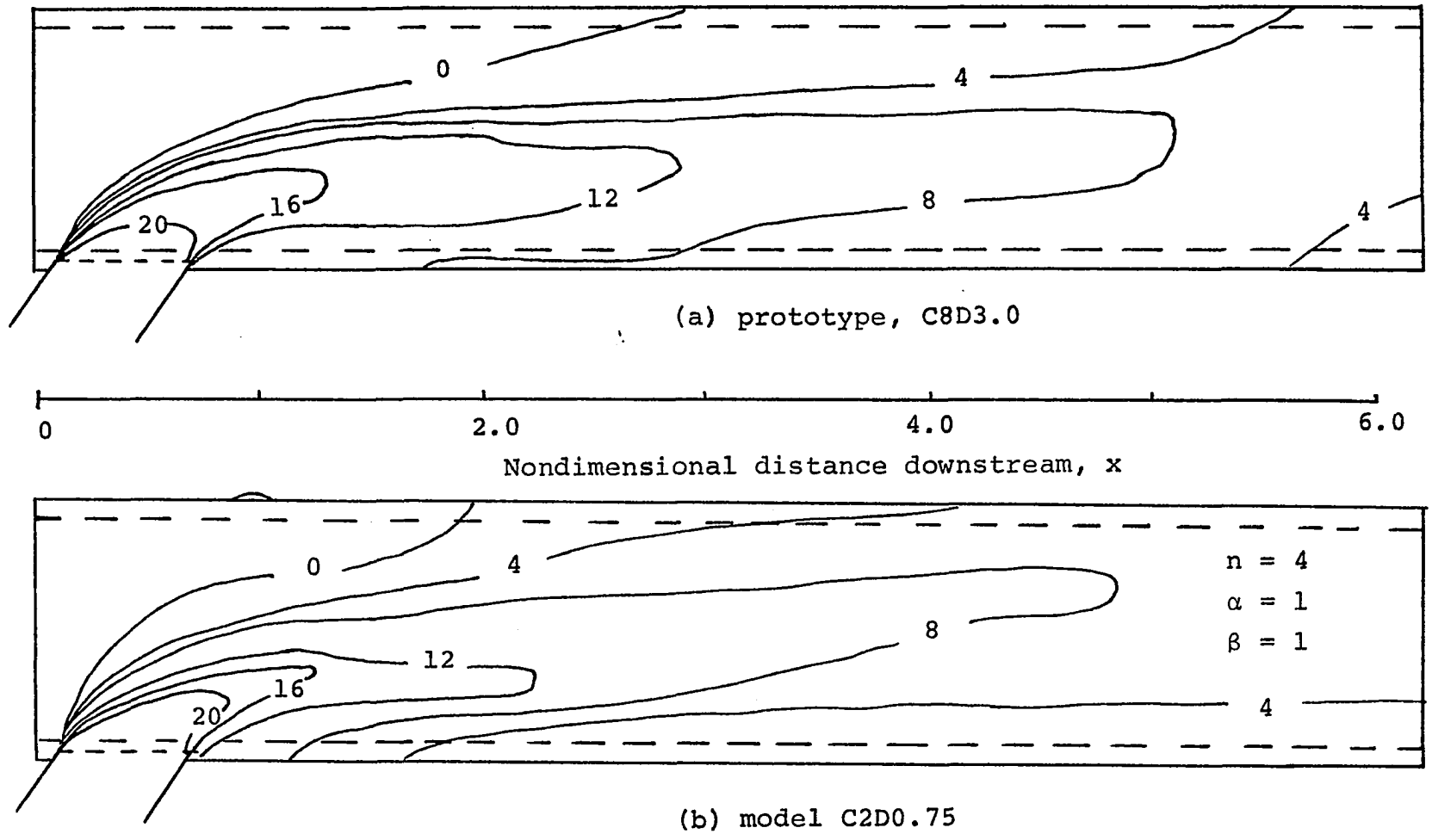

Figure 5. Surface Δt' isotherms in °F, for channels a) C8D3.0 and b) C2D0.75

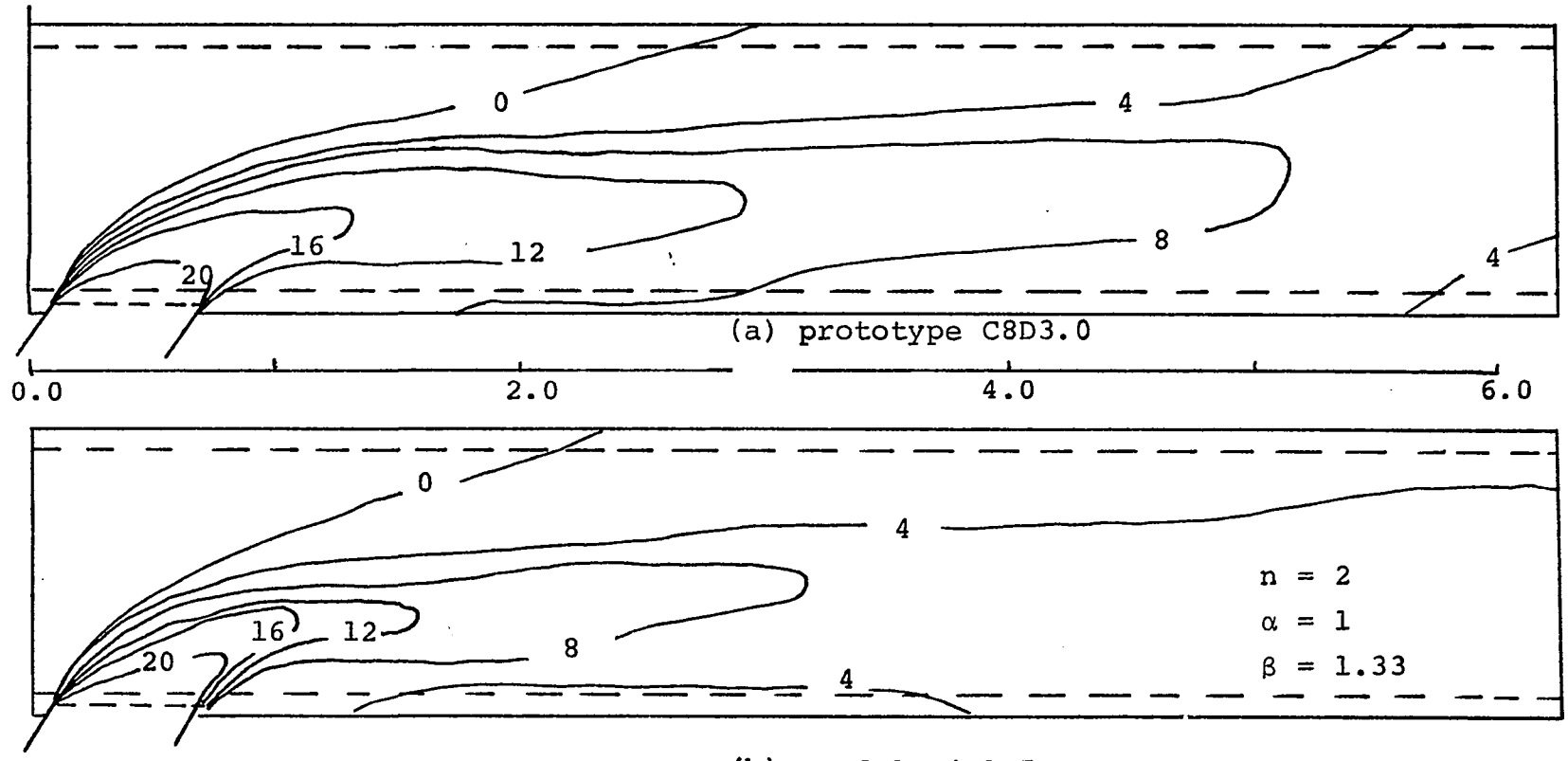

Figure 6. Surface $\Delta t'$ isotherms, in °F, for channels a) C8D3.0 and b) C4D1.5

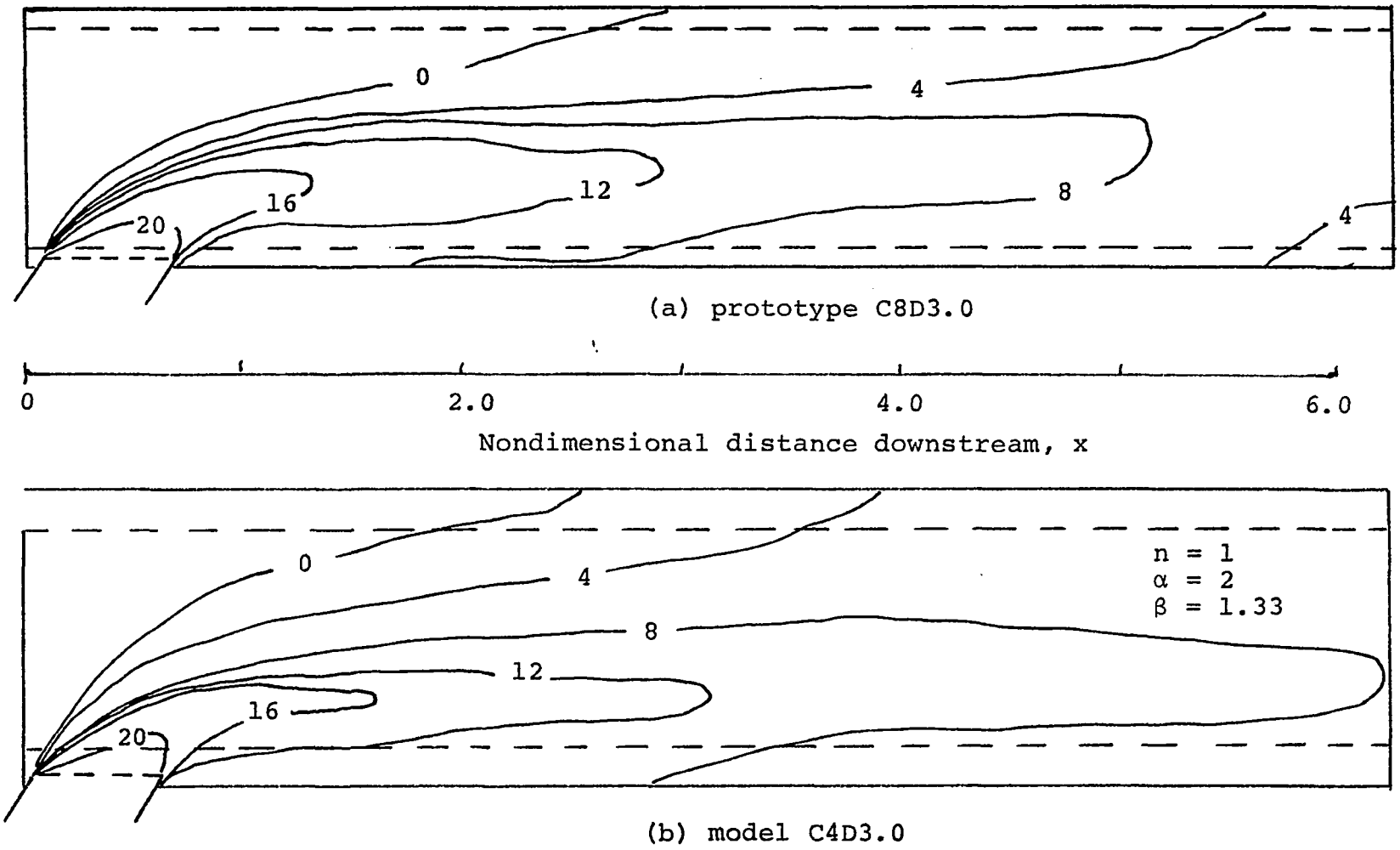

Figure 7. Surface Δt' isotherms, in °F, for channels a) C8D3.0 and b) C4D3.0

To determine if an analytical expression exists a procedure described by Murphy [12] has been used. The procedure is explained and applied in the next section.

B. Prediction Factors for Surface Temperature Differences

To analyze the data it was desirable to be able to define a smooth curve of temperature difference data versus the x coordinate position. Temperature differences of precisely corresponding z coordinates (for example, the channel center line) versus x resulted in excessive scatter, and this scatter masked the trends shown in Figures 5, 6 and 7. To minimize the scatter a maximum temperature difference and an average z temperature difference were defined and used in the analysis.

The maximum temperature difference was taken as the maximum indicated temperature difference for a given x coordinate. The position of this temperature difference versus x traced a line downstream which was nearly the plume centerline. The isotherms tended to be symmetrical about the plume centerline. As was discussed in the preliminary data analysis section the position of the plume centerline does not always correspond exactly in model and prototype. However, for purposes of the data analysis, maximum temperature differences in model and prototype at corresponding x coordinates are assumed to be spatially corresponding temperature differences.

The average z temperature difference is defined as the difference between the average temperature of a small volume element of length dx, depth dz and a width equal to the top width, and the main stream ambient temperature.

The data has first been analyzed to determine the relation of the channel slope distortion to the maximum temperature difference prediction factor for prototype-model situations where no depth distortion occurs.

Maximum temperature differences versus the x coordinate position for various channels are shown in Figures 8, 9, and 10. The slopes of the various channels are listed in Table VI.

There was no slope distortion for the prototype-model combination of C8D3.0-C2D0.75 shown in Figure 8; and over the distance of x = 2.0 to x = 6.0 there is close correspondence (namely a deviation of approximately 1°F or less) between the model and prototype maximum temperature differences. For the prototype-model combination of C8D3.0-C4D1.5 where slope distortion did exist the data in Figure 8 indicates a lack of close correspondence. The data shown in Figure 9 for prototype-model combination C4D2.25-C2D1.13 shows a lack of close correspondence over a range of x = 2.0 to x = 4.0 and again there was slope distortion. The data shown in Figure 10 for prototype-model combination C4D3.0-C2D1.5 shows close correspondence over a range of x = 2.5 to x = 6.0, and there was no slope distortion for this combination. The data from Figures 8, 9, and 10 has been used to determine the expression for δ as a

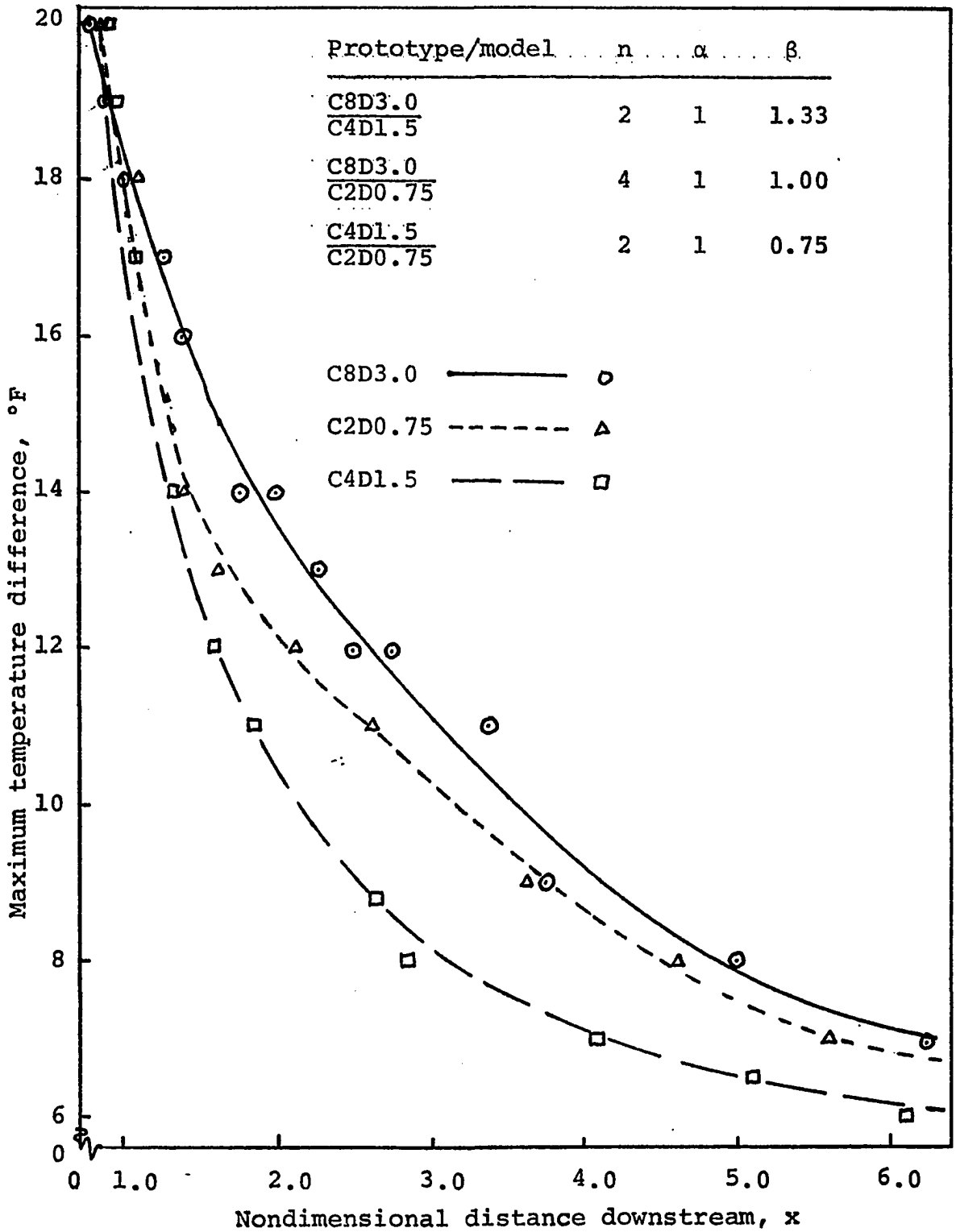

Figure 8. Maximum temperature difference as a function of x for channels C8D3.0, C4D1.5, and C2D0.75

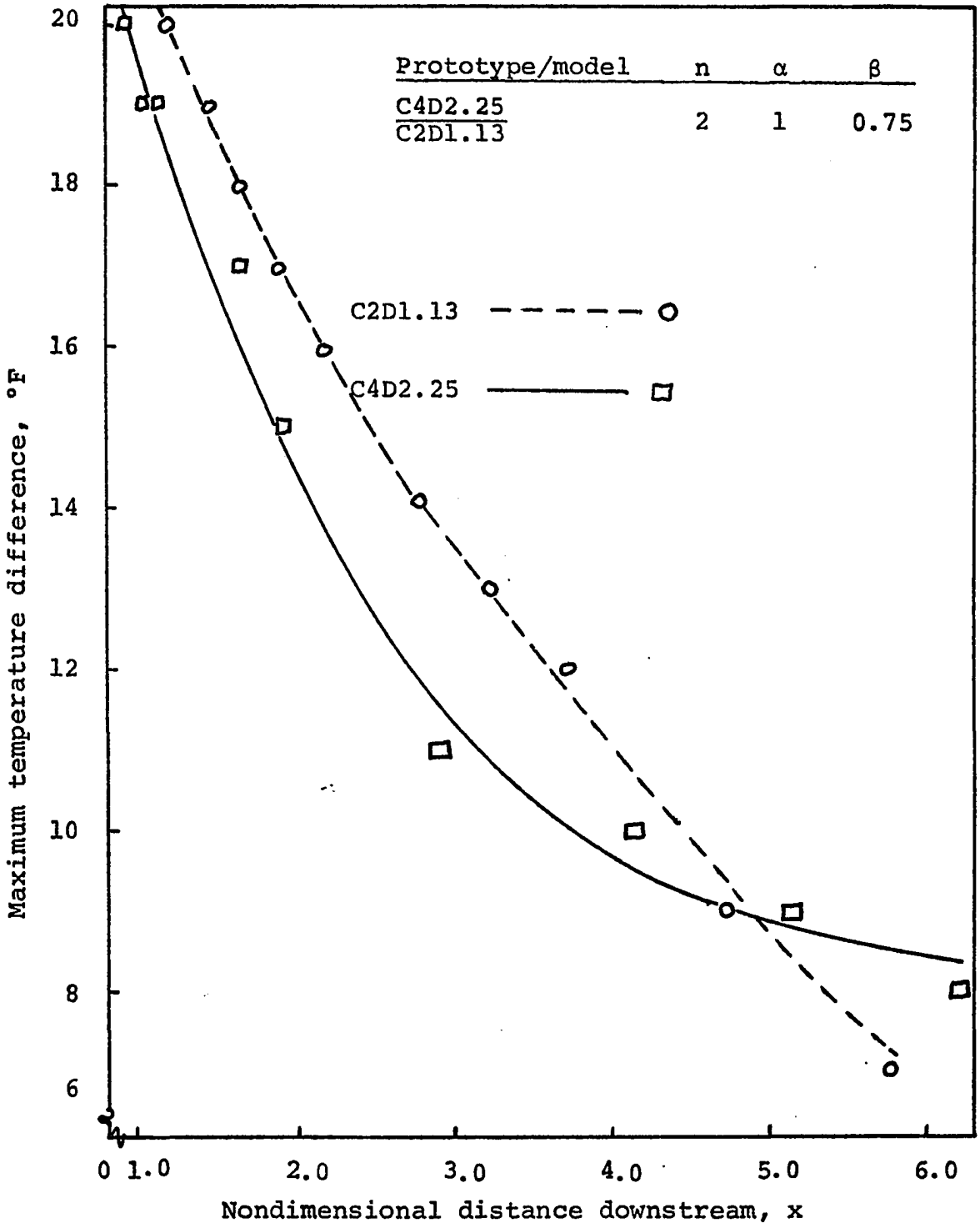

Figure 9. Maximum temperature difference as a function of x for channels C4D2.25 and C2D1.13

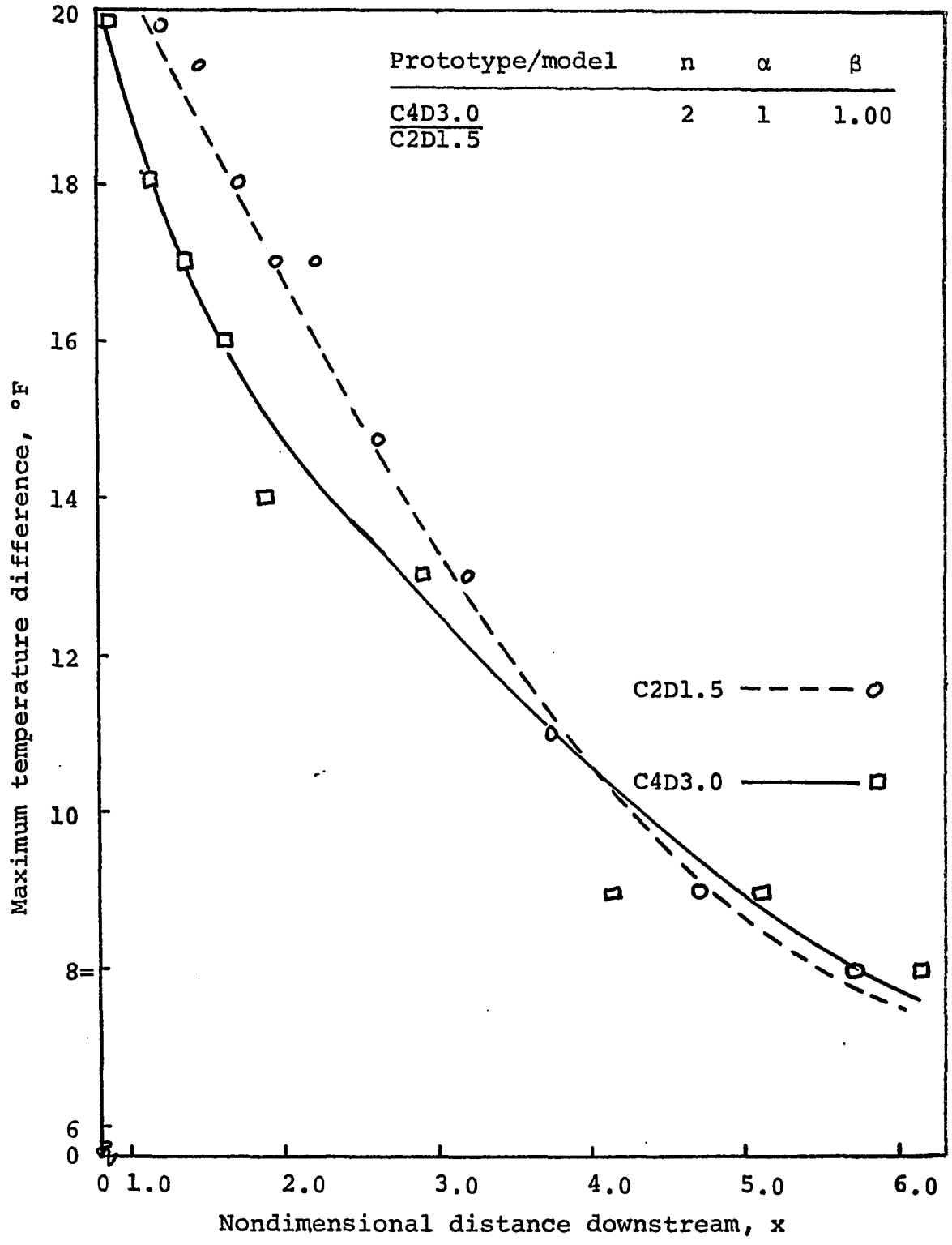

Figure 10. Maximum temperature difference as a function of x for channels C4D3.0 and C2D1.5

Table VI. Temperature differences and channel slopes

Channel	Maximum temperature difference at x = 2.5	Channel bottom slope
C8D3.0	12.2	0.00195
C4D1.5	9.0	0.00260
C4D2.25	12.5	0.00260
C4D3.0	13.6	0.00260
C2D0.75	11.2	0.00195
C2D1.13	14.6	0.00195
C2D1.5	14.9	0.00260

Table VII. Prediction factors, δ_1', distortion factors and length scales

Combination $\left(\frac{\text{Prototype}}{\text{Model}}\right)$	n	α	Experimental prediction factor, δ_1'	β
$\frac{\text{C8D3.0}}{\text{C4D1.5}}$	2	1	1.35	1.33
$\frac{\text{C4D1.5}}{\text{C2D0.75}}$	2	1	0.80	0.75
$\frac{\text{C4D2.25}}{\text{C2D1.13}}$	2	1	0.86	0.75
$\frac{\text{C4D3.0}}{\text{C2D1.5}}$	2	1	0.91	1.0
$\frac{\text{C8D3.0}}{\text{C2D0.75}}$	4	1	1.09	1.0

function of β and n. For the temperature differences at x = 2.5 experimental prediction factors

$$\delta_1(x = 2.5) = \delta_1' = \frac{\Delta t'}{\Delta t_m'} = \frac{\text{Maximum temperature difference in the prototype}}{\text{Maximum temperature difference in the model}}$$

are given in Table VII along with the slope distortion and length scale.

To determine how δ_1', β and n are related, it has been assumed that

$$\delta_1' = \delta_1(x = 2.5) = F(\beta, n) \tag{53}$$

The component equations are

$$(\delta_1')_{\bar{n}} = f_1(\beta, \bar{n}) \tag{54}$$

and

$$(\delta_1')_{\bar{\beta}} = f_2(\bar{\beta}, n) \tag{55}$$

where the bar over the variable denotes a constant value. Then, assuming that Equations (54) and (55) can be combined by multiplication, Equation (53) can be written as

$$\delta_1' = C(\delta_1')_{\bar{n}} \, (\delta_1')_{\bar{\beta}} \tag{53a}$$

where

$$C = \frac{1}{F(\bar{\beta}, \bar{n})} \tag{56}$$

Equation (53a) can be validated by determining a new component equation

$$(\delta_1')_{\bar{\bar{\beta}}} = f_2(\bar{\bar{\beta}}, n) \tag{55a}$$

for $\bar{\bar{\beta}}$, different than $\bar{\beta}$. Another expression similar to Equation (53a) can be formed;

$$\delta_1' = C'(\delta_1')_{\bar{n}} \; (\delta_1')_{\bar{\bar{\beta}}} \tag{53b}$$

where

$$C' = \frac{1}{F(\bar{\bar{\beta}}, \bar{n})} \tag{56a}$$

If Equations (53a) and (53b) are identical then Equation (53a) is valid.

Using the information from Table VII, Equation (54) has been determined from the data plotted in Figure 11. Based on the experimental information from Figures 8 and 10 it will be assumed that for no slope distortion, namely when $\beta = 1$, $\delta_1' = 1$. A straight line approximation for the experimental data in Figure 11 assuming that the line should pass through $(\delta_1')_{\bar{n}} = \beta = 1$ is

$$(\delta_1')_{\bar{n}} = \beta \tag{54a}$$

The data used to develop Equations (52) and (55) is shown in Figures 12 and 13. Approximations for Equations (55) and (55b) are

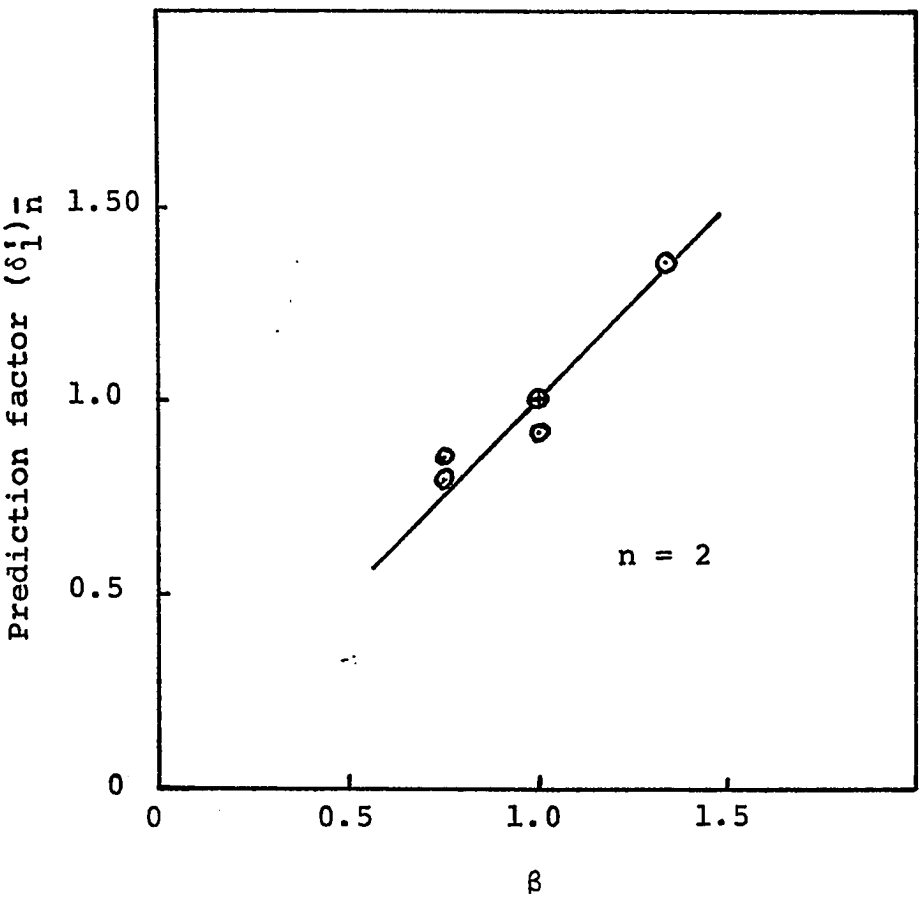

Figure 11. Prediction factor $(\delta_1')_{\bar{n}}$ as a function of β for n = 2

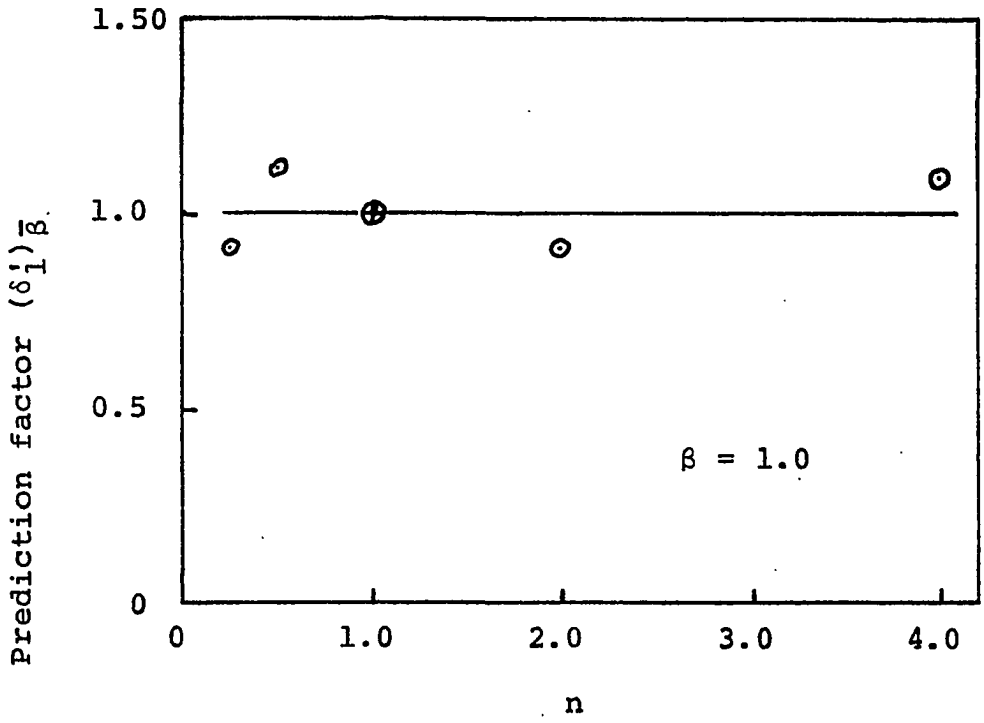

Figure 12. Prediction factor $(\delta_1')_{\bar{\beta}}$ as a function of n for $\beta = 1.0$

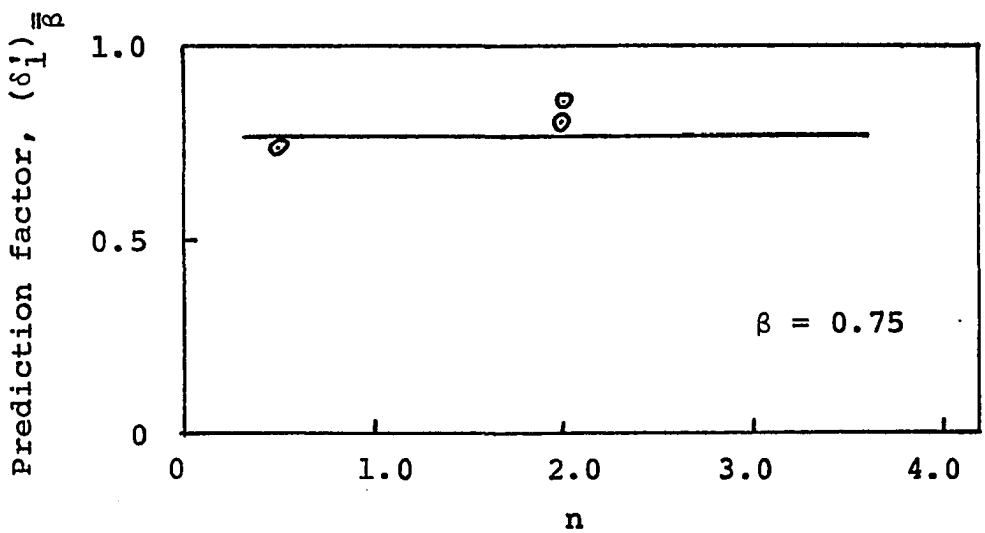

Figure 13. Prediction factor $(\delta_1')_{\bar{\beta}}$ as a function of n for $\beta = 0.75$

$$(\delta_1')_{\bar{\beta}} = 1.0 \tag{55c}$$

$$(\delta_1')_{\bar{\bar{\beta}}} \simeq 0.76 \tag{55d}$$

From Figure 11 for $\beta = 1.0$

$$C = \frac{1}{F(\bar{\beta},\bar{n})} = 1.0 \tag{56b}$$

and substituting Equations (54a) and (55c) into Equation (53a), yields

$$\delta_1' = C(\delta_1')_{\bar{n}}(\delta_1')_{\bar{\beta}} \tag{53c}$$

$$= (1.0)(\beta)(1.0)$$

$$= \beta$$

To validate Equation (53c) another value for C_1', at $\beta = 0.75$ is obtained from Figure 11; namely

$$C' = \frac{1}{F(\bar{\bar{\beta}},\bar{n})} = \frac{1}{0.75} \tag{56c}$$

Equations (54a) and (55d) can be substituted into Equation (53b), and

$$\delta_1' = C'\ \beta(0.75)$$

$$= \left(\frac{1}{0.75}\right)(\beta)(0.76) \tag{53d}$$

$$\simeq \beta$$

Equation (53d) is identical to Equation (53c) and therefore Equation (53c) is a valid expression. Equation (53c) indicates that the prototype-model maximum temperature difference ratio is inversely proportional to the prototype-model slope ratio.

Some subjective judgment was used in establishing Equations (54a), (55c), and (55d) by forcing the function to pass through a given coordinate and in selecting the slope of the straight line. The resulting expression, Equation (53c), has been assumed to be a satisfactory approximation of the experimental data.

Equation (53c) has been developed from data for values of $n = 0.25$ to $n = 4.0$ and of $\beta = 0.67$ to $\beta = 1.33$. Equation (53c) will be used for β in the range of $\beta = 0.5$ to $\beta = 2.0$. It will be assumed that Equation (53c) remains valid for this range.

In the following paragraphs Equation (53c) will be used to adjust certain experimentally determined maximum temperature differences. Usually this adjustment implies an increase in channel slope. To maintain uniform flow at the proper depth with the increased slope, the channel surface would require roughening. It will be assumed that this added roughness would not alter the validity of Equation (53c). This would seem to be a reasonable assumption since adding roughness as slope is increased should generate additional turbulence which would increase dispersion and lower the temperature difference. The

converse of higher temperature differences with slope reductions and corresponding surface roughness reduction is also assumed to be valid.

To determine if Equation (53c) was valid for other x values, Equation (53c) was used to adjust model data to obtain temperature differences that correspond to a model operating at the proper slope. The combination C8D3.0-C4D1.5 was selected first. Channel C8D3.0 was considered the prototype. If design conditions had been met there would have been no slope distortion, namely $\beta = 1$; however, the experimental situation resulted in $\beta = 1.33$.

To correct the C4D1.5 data, a second combination of C4D1.5 at its actual slope as the prototype, and C4D1.5 at its desired slope as the model was used. The slope ratio for this combination was

$$\beta' = \frac{.00195}{.00260} = 0.75$$

Then from Equation (53c)

$$\frac{\text{C4D1.5 experimental maximum temperature difference}}{\text{C4D1.5 adjusted maximum temperature difference}} = \frac{\Delta t'}{\Delta t'_m} = \beta' = 0.75$$

and

$$\Delta t'_m = \frac{\Delta t'}{0.75}$$

The adjusted values for C4D1.5 are shown in Figure 14, and it is shown that Equation (53c) provides a satisfactory adjustment at x = 2.5 as well as a close correspondence to the

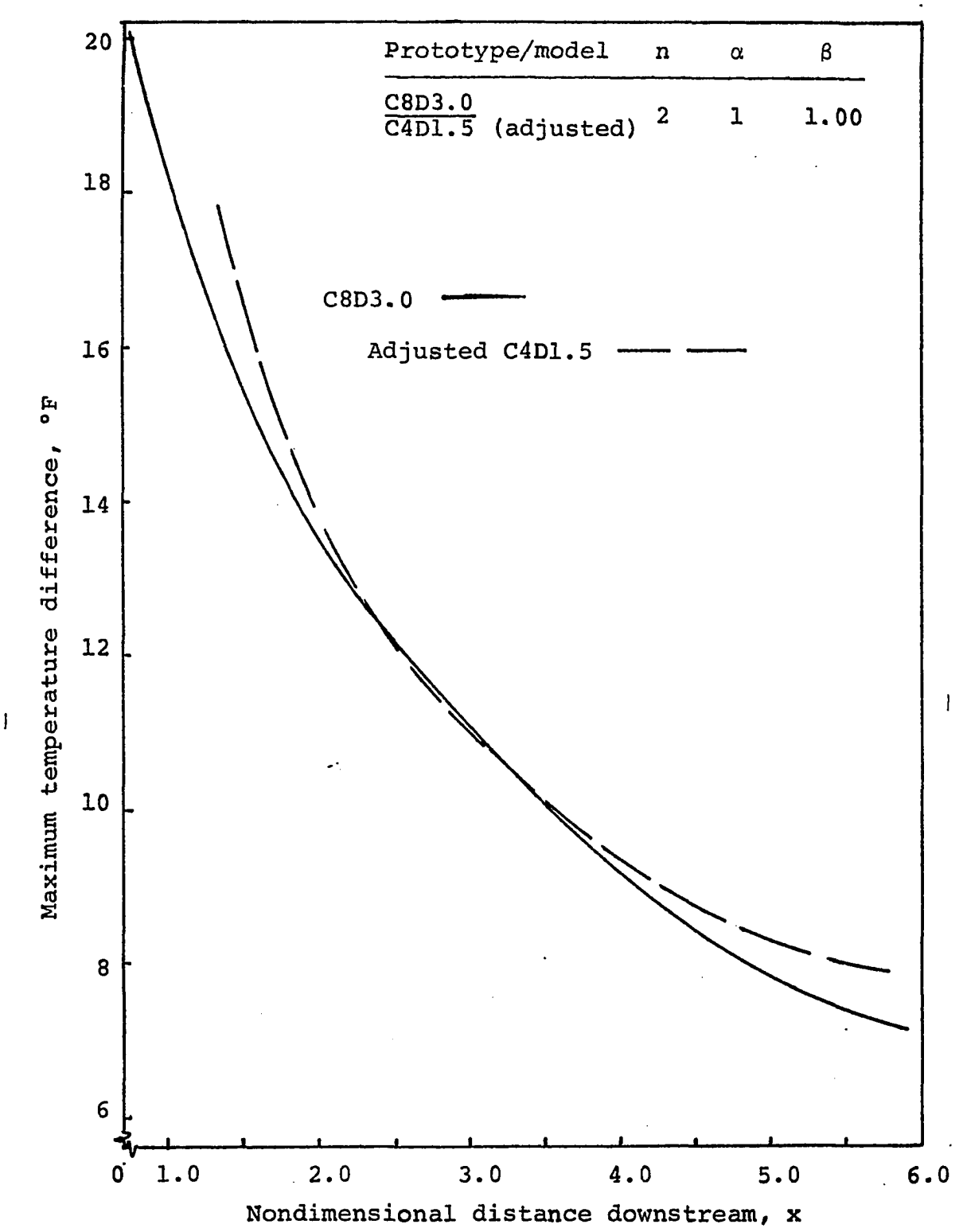

Figure 14. Maximum temperature difference as a function of x for C8D3.0, and for the adjusted data of C4D1.5

prototype, C8D3.0, over the range x = 1.5 to x = 5.5.

The data adjustment procedure has been applied to the C2D1.13 data in Figure 9. In this instance C2D1.13 was operated at a slope that was 75% of that dictated by design conditions with C4D2.25 as the prototype. To correct the data the experimental data for C2D1.13 was considered the prototype situation, and C2D1.13 operating at the same slope as C4D2.25 was considered the model. Then

$$\beta' = 1.33$$

and

$$\Delta t_m = \frac{t}{1.33}$$

The adjusted data is plotted in Figure 15, and the deviation has been reduced over a range of x = 2.0 to x = 3.5. The adjustment does not result in a close correspondence over a large range. Maximum temperature differences for C2D1.13 might have been low because of thermistor probe spacing. The centerlines of the thermistors for C2D1.13 were 0.4 inches apart, but this represented a relative spacing of $\Delta z = 0.20$ and higher peak temperatures may have been missed. The relative spacing for the thermistors for C4D2.25 was $\Delta z = 0.125$ and this provided a finer grid.

To study the effect of depth distortion on prediction factors, the experimentally determined maximum temperature differences of many of the models were adjusted to obtain a temperature difference that was associated with a channel

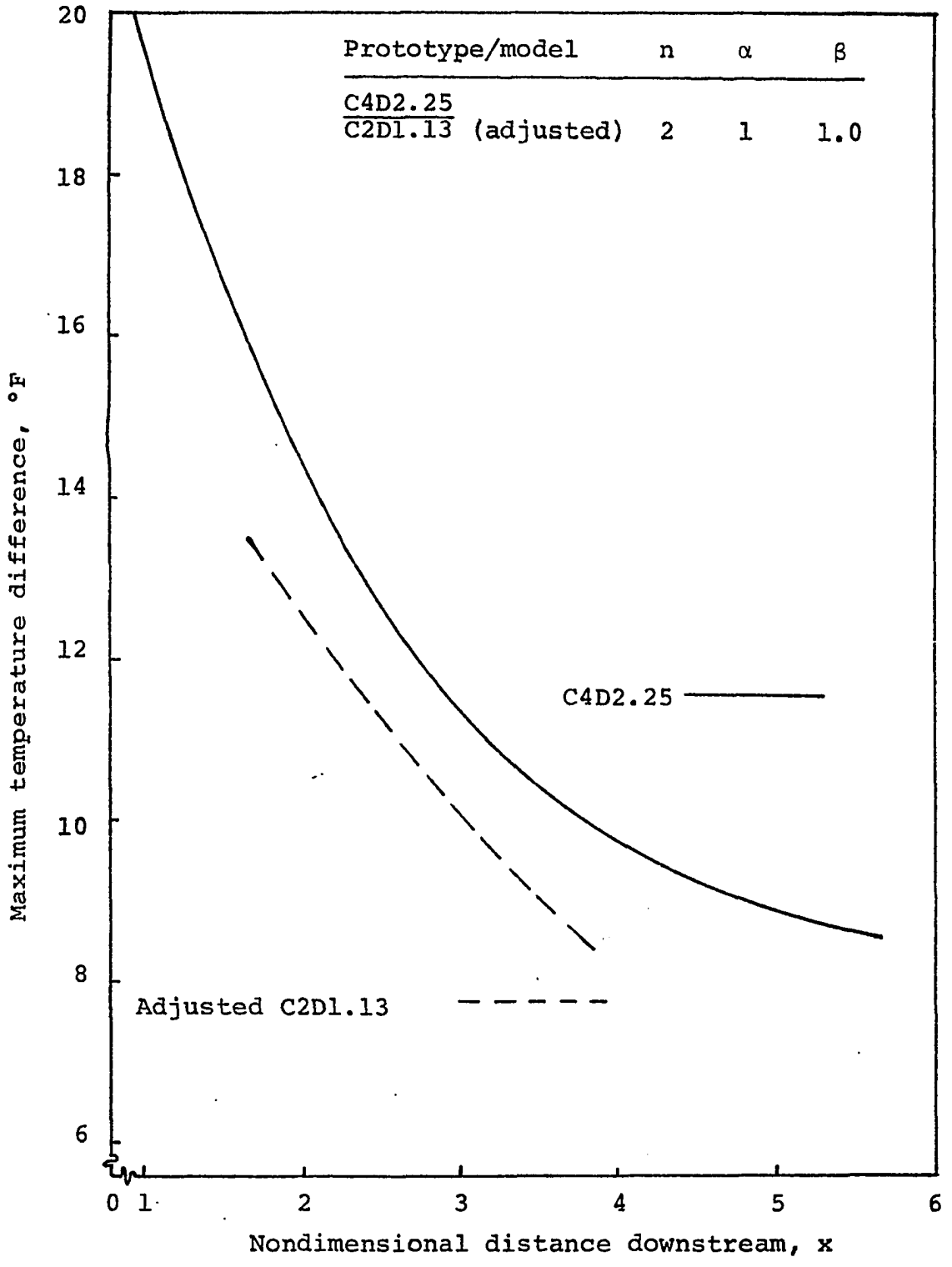

Figure 15. Maximum temperature difference as a function of x for C4D2.25 and for the adjusted data of C2D1.13

operating at a slope required by design conditions.

The adjusted maximum temperature differences were obtained by using the procedure described for the adjusted data in Figure 14. The adjusted temperature difference was an average of two computations. For example, to compute the adjusted maximum temperature difference for C4D2.25 one prototype was C4D2.25 at its actual slope and a second prototype was C2D1.13 at its actual slope. For both prototypes the model was C4D2.25 at the slope dictated by design conditions for the value of α involved. Thus each average that was computed involved one channel where n = 1 and a second channel where n = 2 or n = 0.5.

The temperature difference ratios, δ_2'

$$\delta_2 = \frac{\Delta t'}{\Delta t_m'} = \frac{\text{maximum temperature difference in prototype}}{\text{maximum temperature difference in model (with model operating at the slope required by design conditions)}}$$

with

$$\delta_2(x = 2.5) = \delta_2'$$

for various prototype-model combinations computed from the adjusted data, are listed in Table VIII along with the depth distortion factors and the length scales.

The relation between δ_2', β and n for depth distorted models was determined by using the same procedures as used before to develop the relation between δ_1', β and n.

Table VIII. Prediction factors δ_2', distortion factors and length scale

Combination Prototype / Model	Prediction factor, δ_2'	n	α^a
C8D3.0 / C4D2.25	1.16	2	1.5
C8D3.0 / C4D3.0	1.28	2	2.0
C4D1.5 / C2D1.13	1.15	2	1.5
C4D1.5 / C2D1.5	1.27	2	2.0
C8D3.0 / C2D1.13	1.16	4	1.5
C8D3.0 / C2D1.5	1.28	4	2.0
C4D2.25 / C2D1.5	1.22	2	1.33
C4D1.5 / C4D3.0	1.18	1	2.0
C2D0.75 / C2D1.13	1.02	1	1.5
C2D0.75 / C2D1.5	1.35	1	2.0
C4D3.0 / C2D1.5	0.90	2	1.0
C4D1.5 / C4D2.25	1.15	1	1.5

[a] $\beta = \alpha$.

It was assumed that

$$\delta_2' = F(\alpha, n)$$
$$= C(\delta_2')^{-}_{n}(\delta_2')^{-}_{\alpha} \quad (57)$$

The component equations are

$$(\delta_2')^{-}_{n} = f(\alpha, \bar{n}) \quad (58)$$

and

$$(\delta_2')_{\bar{\alpha}} = f\ (\bar{\alpha}, n) \tag{59}$$

The data for Equation (58) is shown in Figure 16 and, assuming that the function should pass through $(\delta_2')_{\bar{n}} = \alpha = 1$, a straight line approximation for Equation (58) is

$$(\delta_2')_{\bar{n}} = 0.70 + 0.30\alpha \tag{58a}$$

The data for Equation (59), shown in Figure 17, yields

$$(\delta_2')_{\bar{\alpha}} = 1.15 \tag{59a}$$

From Figure 16 for $\alpha = 1.5$

$$C = \frac{1}{F(\bar{\alpha},\bar{n})} = 1.16 \tag{60}$$

and substituting Equations (58a) and (59a) and (60) into Equation (57) yields

$$\delta_1' = \frac{(0.70 + 0.3\alpha)(1.15)}{1.16} \simeq 0.70 + 0.30\alpha \tag{57a}$$

This expression was validated by developing a second expression for Equation (59) using data plotted in Figure 18; namely,

$$(\delta_2')_{\bar{\alpha}} = 1.27 \tag{59b}$$

From Figure 16 for $\alpha = 2.0$

$$C' = \frac{1}{f(\bar{\bar{\alpha}},\bar{n})} = 1.25 \tag{60a}$$

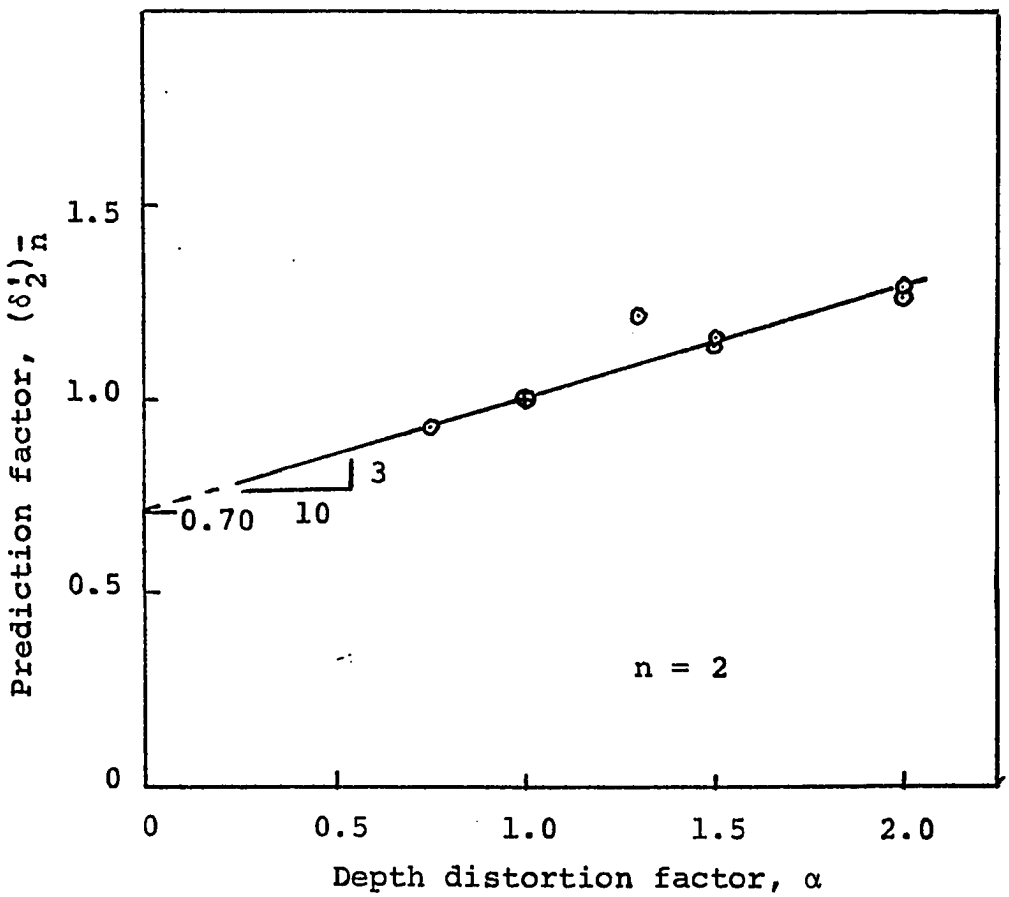

Figure 16. Prediction factor $(\delta_2')_{\bar{n}}$ as a function of α for n = 2

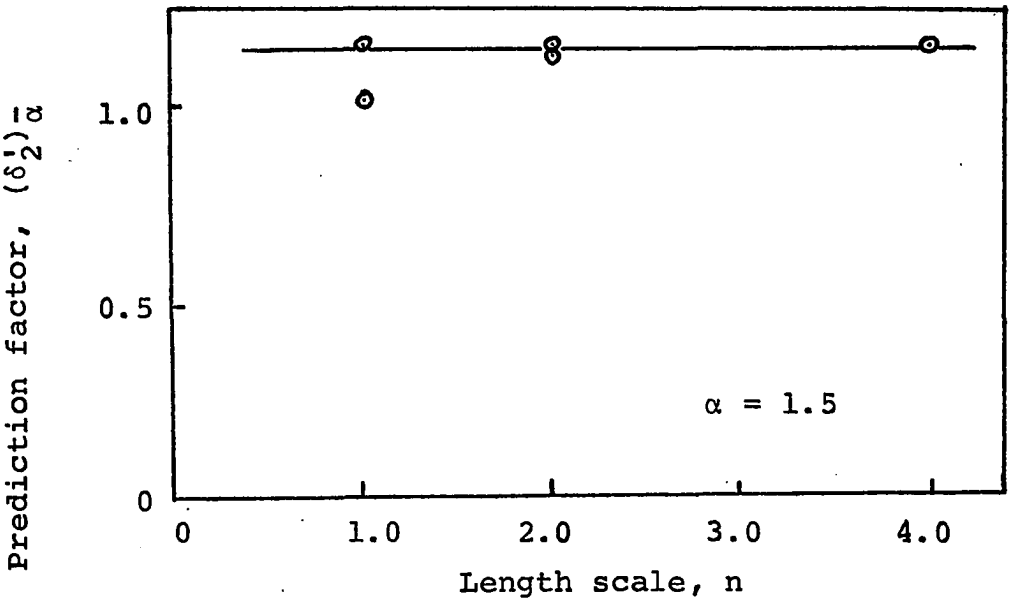

Figure 17. Prediction factor $(\delta_2')_{\bar{\alpha}}$ as a function of n for α = 1.5

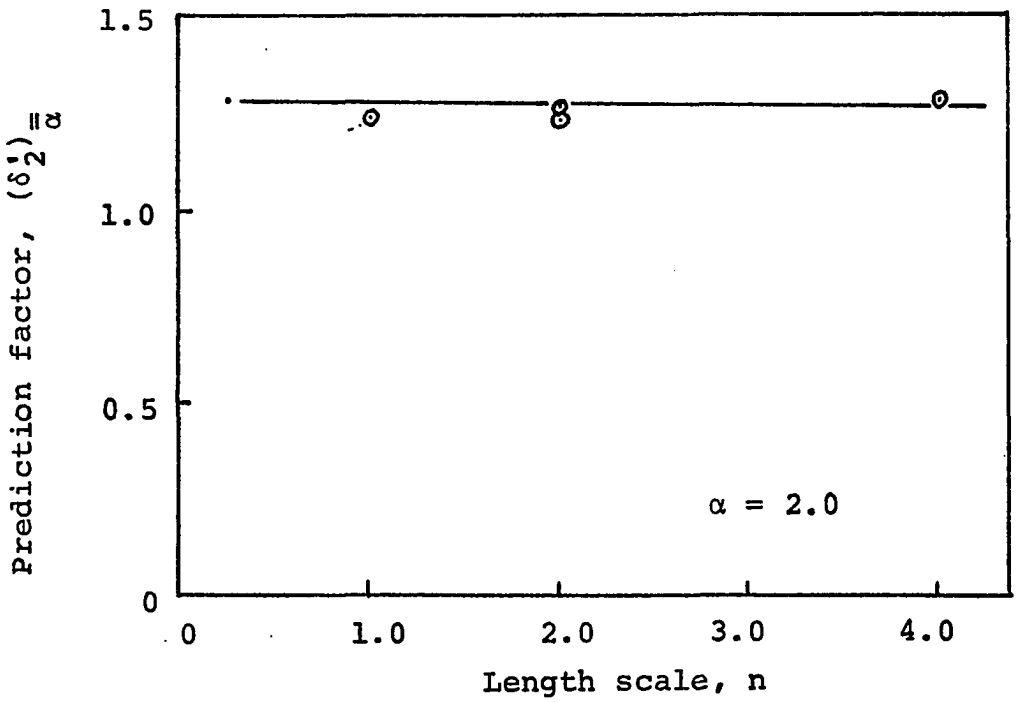

Figure 18. Prediction factor $(\delta_2')_{\bar{\bar{\alpha}}}$ as a function of n for α = 2.0

and substituting Equations (58a), (59b) and (60a) into Equation (57), yields

$$\delta_2' = (0.70 + 0.30\alpha)\,\frac{1.27}{1.25}$$

$$\simeq 0.70 + 0.30\alpha \qquad (57b)$$

Equation (57b) is identical to Equation (57a) and thus Equation (57a) is validated. Equation (57a) expresses the relation between the depth distortion and the prediction factor for models that are operated at the slope dictated by design conditions. With no distortion, namely $\alpha = 1$, Equation (57a) yields $\delta_2' = 1$ as would be expected.

Average z temperature differences were selected for analysis because they enabled definition of a smooth curve of temperature difference data versus x and, also because they could be used to help approximate temperatures at specific z coordinates.

Average surface temperatures have been computed by creating a number of volume cells across the surface, associating a given temperature with each cell and then determining the average temperature of the cells. The x and y dimensions of the cell were considered small increments, and the z dimension of the cell was equal to the distance between thermistor probes. Each cell was centered at the position of a thermistor except for the outer two cells so that the temperature indicated by

the thermistor was taken as the average cell temperature. The total number of cells, e, was equal to the surface top width divided by the cell width.

The average temperature was computed from

$$\overline{\Delta t'} = \frac{\Sigma \text{ Vol.}_{cell}}{\text{Vol.}_{total}} \times \Delta t'_{cell} = \frac{\Sigma \Delta t'}{e} \qquad (61)$$

where

$$\text{Vol.}_{total} = e \times \text{Vol.}_{cell}$$

Where partial cells were encountered at edges the volume adjustment was transferred to the cell temperature; namely

$$((\text{Cell fraction}) \times \text{Vol.}_{cell}) \times \Delta t'_{cell} =$$

$$(\text{Vol.}_{cell}) \times (\text{Cell fraction} \times \Delta t'_{cell})$$

The top width of Channels C4D2.25, C4D3.0, C2D1.13, C2D1.5 were distorted for combinations where they were models and $\alpha \neq 1$ because the slope of the channel sides was fixed and could not be changed as dictated by the distortion of the vertical dimensions. In such cases the model top width was reduced to the length required by horizontal length design conditions for computing the number of cells. This resulted in the two outer cells used in the computation of the average temperature difference being slightly smaller in volume than the actual cell.

The average z temperature differences for the various channels are shown in Figures 19, 20, and 21. The slopes for the channels are listed in Table IX. The average z temperature differences show approximately the same relationship to each other as did the maximum temperature differences but over the smaller range of x = 2.5 to x = 6.0.

The same procedure has been used for developing the relation between average temperature difference ratios and β, α and n as was used for the maximum temperature difference data. The average z temperature difference ratios

$$\delta_3(x = 2.5) = \delta_3' = \frac{\text{average z temperature difference, prototype}}{\text{average z temperature difference, model}}$$

for the various prototype-model combinations with no depth distortion are listed in Table X. It has been assumed that

$$\delta_3' = F(\beta, n)$$

$$= C(\delta_2')_{\bar{n}}(\delta_2')_{\bar{\beta}} \tag{62}$$

where the component equations are

$$(\delta_3')_{\bar{n}} = f_1(\beta, \bar{n}) \tag{63}$$

$$(\delta_3')_{\bar{\beta}} = f_2(\bar{\beta}, n) \tag{64}$$

and

$$C = \frac{1}{F(\bar{\beta}, \bar{n})} \tag{65}$$

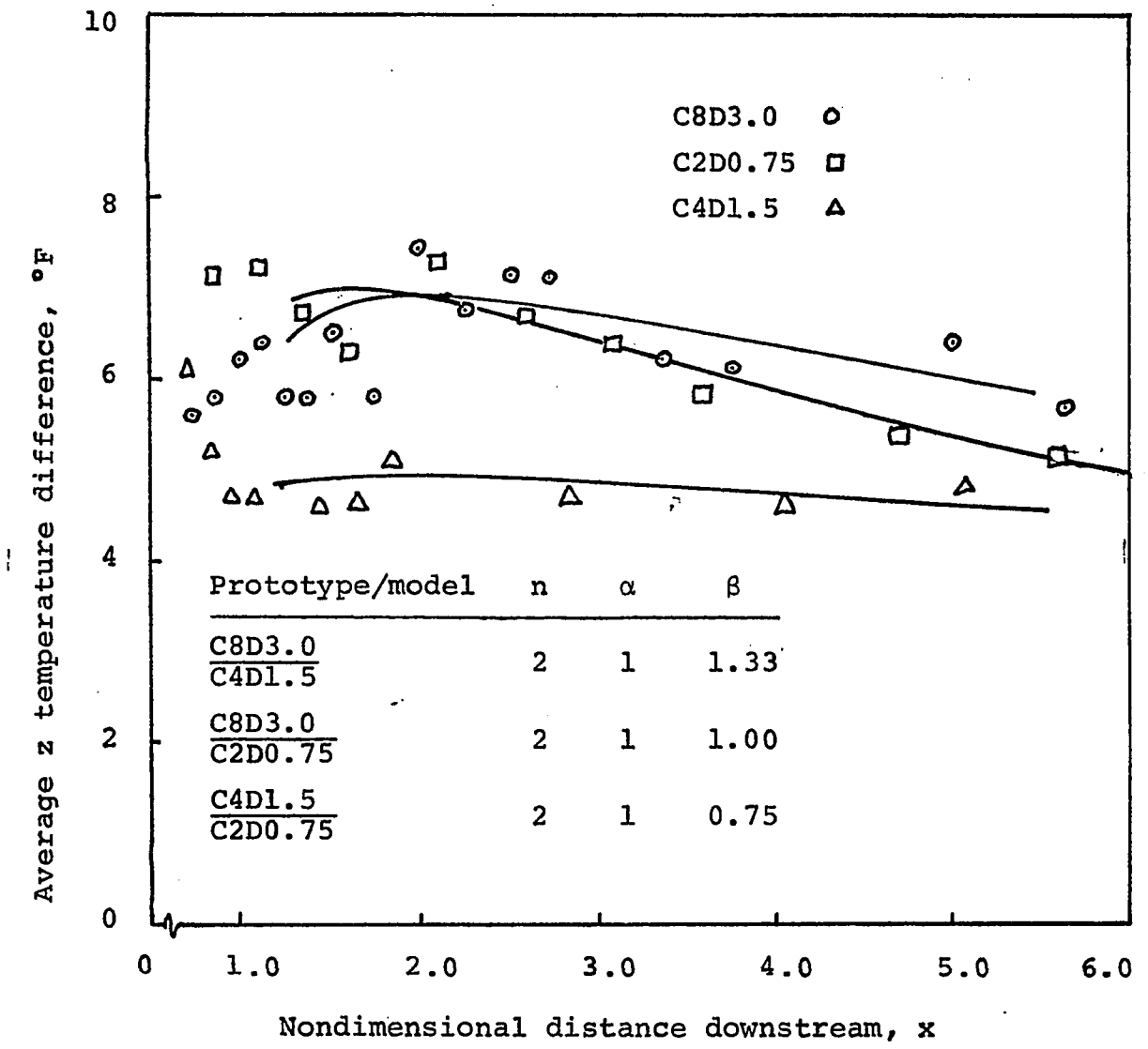

Prototype/model	n	α	β
C8D3.0 / C4D1.5	2	1	1.33
C8D3.0 / C2D0.75	2	1	1.00
C4D1.5 / C2D0.75	2	1	0.75

Figure 19. Average z temperature difference as a function of downstream distance

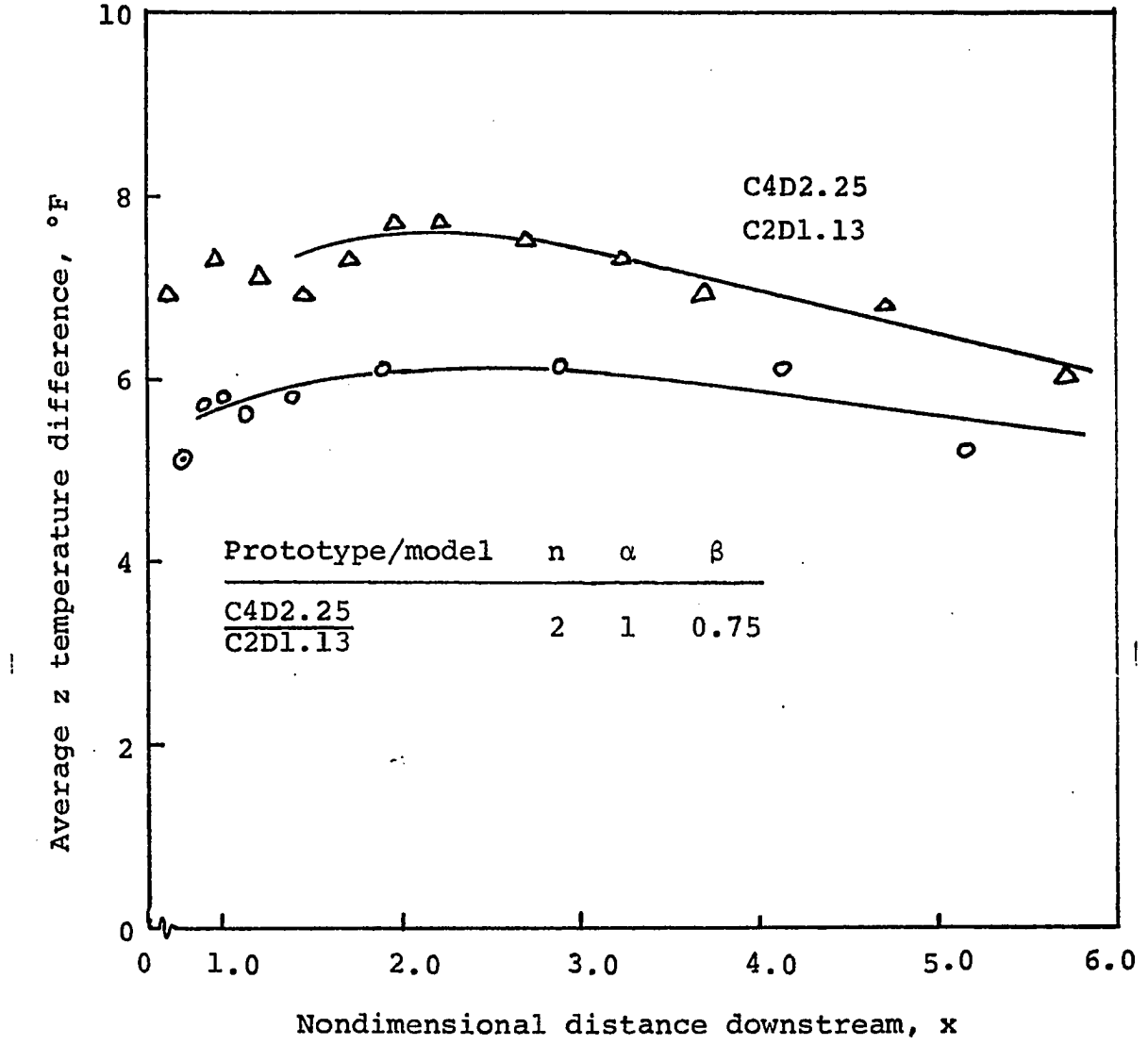

Figure 20. Average z temperature difference function of downstream distance

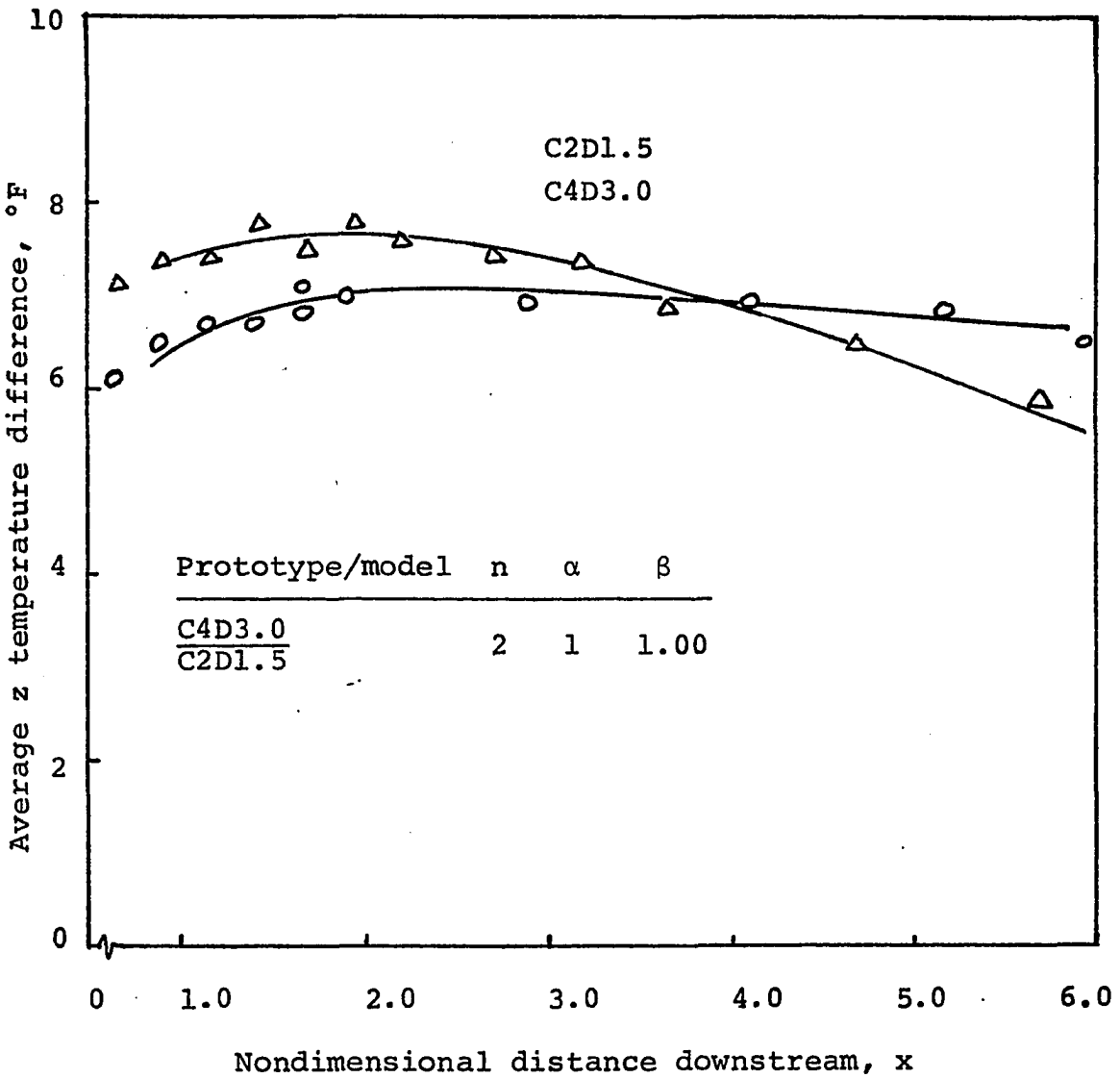

Figure 21. Average z temperature difference as a function of downstream distance

Table IX. Average z temperature differences and channel slopes

Channel	Average z temperature difference at x = 2.5 °F	Channel bottom slope
C8D3.0	6.8	0.00195
C4D1.5	4.9	0.00260
C4D2.25	6.1	0.00260
C4D3.0	7.1	0.00260
C2D0.75	6.7	0.00195
C2D1.13	7.6	0.00195
C2D1.5	7.5	0.00260

Table X. Prediction factors, δ_3^1, distortion factors and length scales

Combination $\left(\frac{\text{Prototype}}{\text{Model}}\right)$	n	α	Experimental prediction factor δ_3	β
$\frac{\text{C8D3.0}}{\text{C4D1.5}}$	2	1	1.38	1.33
$\frac{\text{C8D3.0}}{\text{C2D0.75}}$	4	1	1.01	1.00
$\frac{\text{C4D1.5}}{\text{C2D0.75}}$	2	1	0.73	0.75
$\frac{\text{C4D2.25}}{\text{C2D1.13}}$	2	1	0.80	0.75
$\frac{\text{C4D3.0}}{\text{C2D1.5}}$	2	1	0.95	1.00

The data for Equation (63) is shown in Figure 22.

Assuming that $f_1(\beta,\bar{n})$ should pass through the point

$$(\delta_3')_{\bar{n}} = \beta = 1$$

a straight line approximation for $f_1(\beta,\bar{n})$ is

$$(\delta_3')_{\bar{n}} = \beta \tag{63a}$$

The data for Equation (64) is shown in Figure 23 and yields

$$(\delta_3')_{\bar{\beta}} = 1.00 \tag{64a}$$

From Figure 22 for $\beta = 1$

$$C = \frac{1}{F(\bar{\beta},\bar{n})} = \frac{1}{1} = 1 \tag{65a}$$

Equations (63a), (64a), and (65a) can be substituted into Equation (62) to form

$$\delta_3' = \frac{\beta\ (1)}{1} = \beta \tag{62a}$$

Equation (62a) can be validated by developing a second expression for Equation (64) using the data plotted in Figure 24, namely

$$(\delta_3')_{\bar{\beta}} = 0.75 \tag{64b}$$

From Figure 22, for $\beta = 0.75$

$$C = \frac{1}{F(\bar{\beta},\bar{n})} = \frac{1}{0.75} \tag{65b}$$

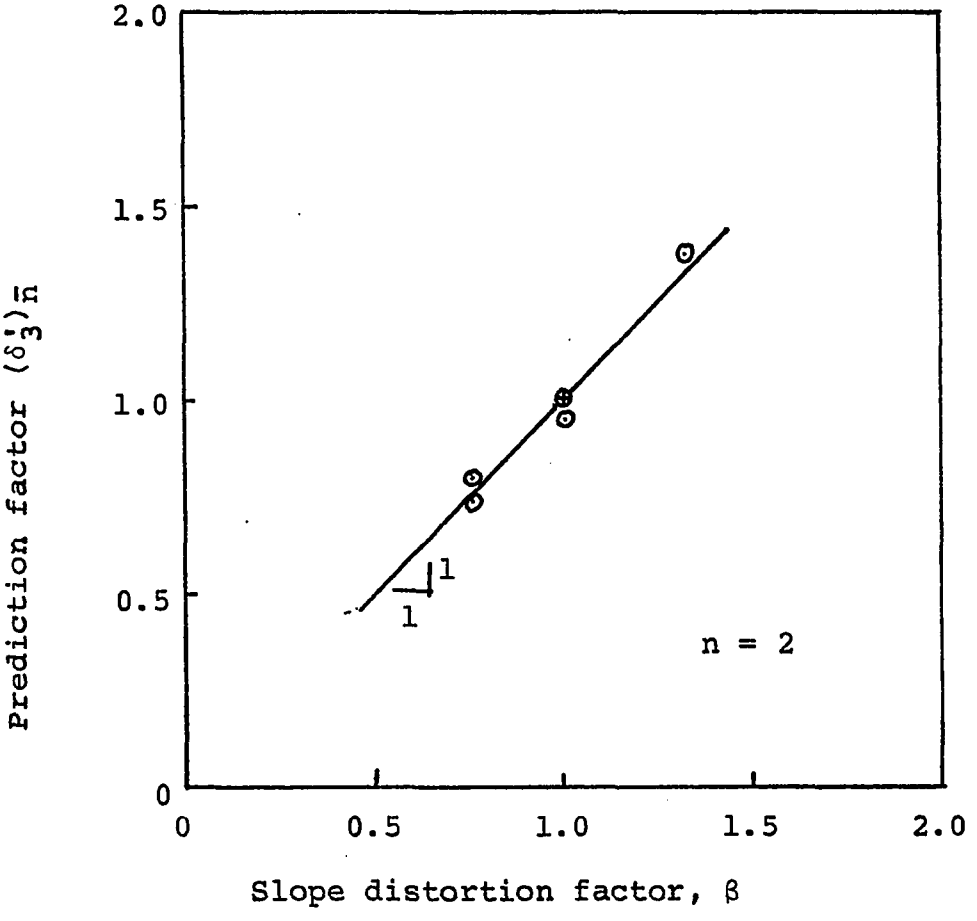

Figure 22. Prediction factor, $(\delta_3')_{\bar{n}}$ as function of β for n = 2

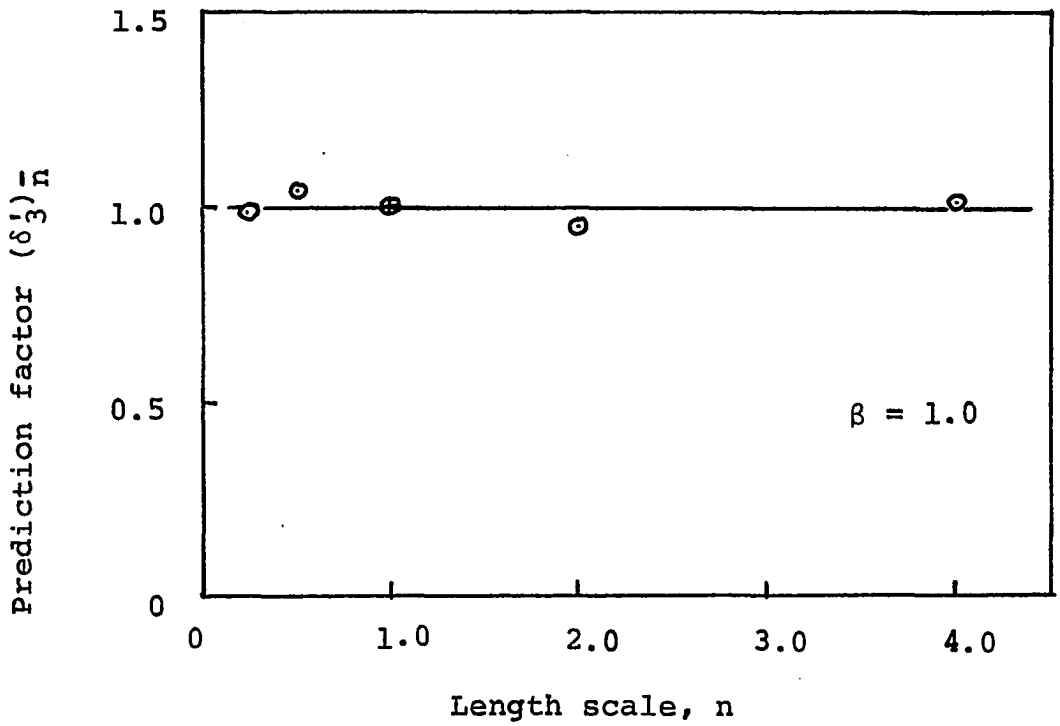

Figure 23. Prediction factor $(\delta_3')_{\bar{n}}$ as a function of n for $\beta = 1.0$

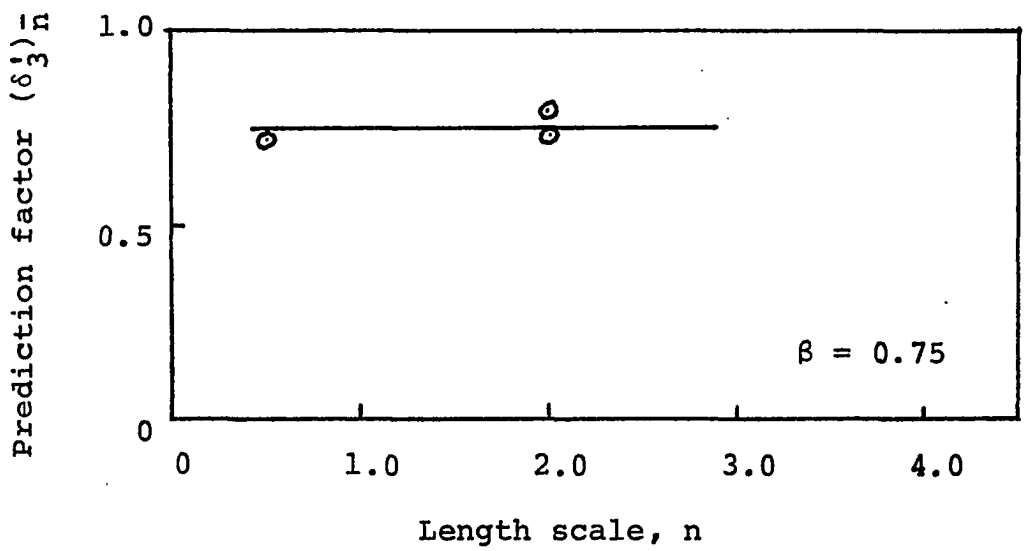

Figure 24. Prediction factor $(\delta_3')_{\bar{n}}$ as function of n for $\beta = 0.75$

Substituting Equations (63a), (64b), and (65b) into Equation (62) yields

$$\delta_3' = \frac{(\beta)(0.75)}{0.75} = \beta \tag{62b}$$

which is identical to Equation (62a) and thus validates Equation (62a).

Equation (62a) can be used to adjust the average temperature difference of the vertical dimension distorted models that were operated at slopes different from design conditions. The adjusted average temperature difference ratios

$$\delta_4(x = 2.5) = \delta_4' = \frac{\text{average z temperature difference, prototype}}{\text{adjusted ave. z temperature difference, model}}$$

are listed in Table XI. It will be assumed that

$$\delta_4' = F(\alpha,n) = C(\delta_4')_{\bar{n}}(\delta_4')_{\bar{\alpha}} \tag{66}$$

where the component equations are

$$(\delta_3')_{\bar{n}} = f_1(\alpha,\bar{n}) \tag{67}$$

$$(\delta_3')_{\bar{\alpha}} = f_2(\bar{\alpha},n) \tag{68}$$

and the constant is

$$C = \frac{1}{F(\bar{\alpha},\bar{n})} \tag{69}$$

The data for Equation (67) is plotted in Figure 25. Assuming that $f_1(\alpha,\bar{n})$ should pass through the point $(\delta_3')_{\bar{n}} = \alpha = 1$, a straight line approximation for Equation (67) is

Table XI. Prediction factors, δ_4', distortion factors and length scales

Combination $\left(\frac{\text{Prototype}}{\text{Model}}\right)$	Prediction factor, δ_4'	n	α^a
$\frac{C8D3.0}{C4D2.25}$	1.25	2	1.5
$\frac{C8D3.0}{C4D3.0}$	1.39	2	2.0
$\frac{C4D1.5}{C2D1.13}$	1.11	2	1.5
$\frac{C4D1.5}{C2D1.5}$	1.38	2	2.0
$\frac{C8D3.0}{C2D1.13}$	1.25	4	1.5
$\frac{C8D3.0}{C2D1.5}$	1.36	4	2.0
$\frac{C4D2.25}{C2D1.5}$	1.08	n	1.33
$\frac{C4D3.0}{C2D0.75}$	0.71	2	0.5
$\frac{C4D2.25}{C2D0.75}$	0.81	2	0.67

[a] $\beta = \alpha$.

$$(\delta_4')_{\bar{n}} = 0.65 + 0.35\alpha \tag{67a}$$

The data for Equation (68) for $\alpha = 1.5$ is plotted in Figure 26 and it yields

$$(\delta_4')_{\bar{\alpha}} = 1.18 \tag{68a}$$

From Figure 25 for $\alpha = 1.5$

$$C = \frac{1}{F(\bar{\alpha},\bar{n})} = \frac{1}{1.18} \tag{69a}$$

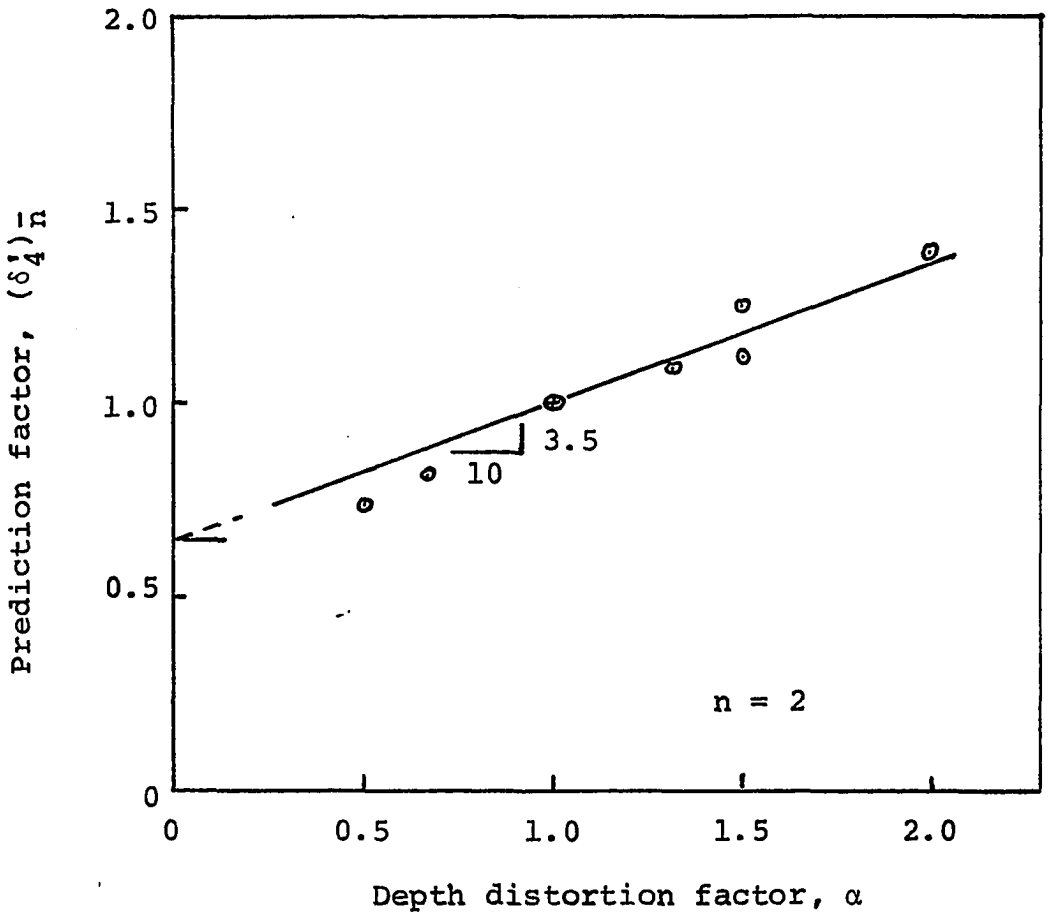

Figure 25. Prediction factor, $(\delta_4')_{\bar{n}}$, as a function of α for n = 2

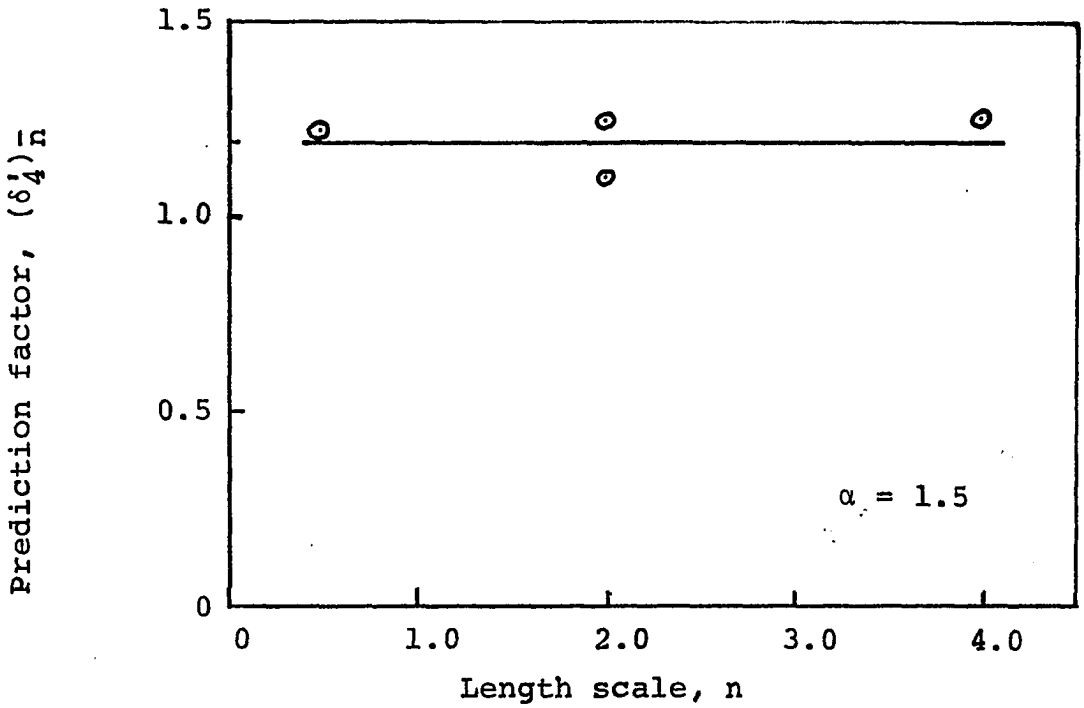

Figure 26. Prediction factor $(\delta_4')_{\bar{n}}$ as a function of n for $\alpha = 1.5$

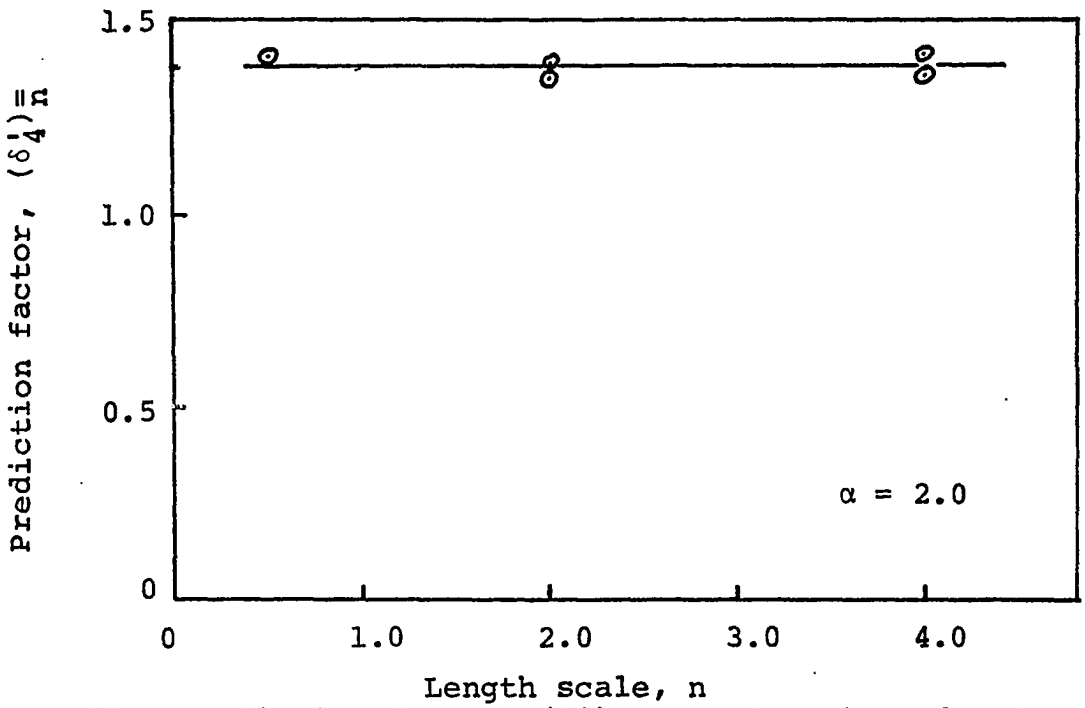

Figure 27. Prediction factor, $(\delta_4')_{\bar{n}}$ as a function of n for $\alpha = 2.0$

Substituting Equations (67a), (68a) and (69a) into Equation (66) yields

$$\delta_4' = (0.65 + 0.35\alpha)\ \frac{1.18}{1.18}$$

$$= 0.65 + 0.35\alpha \qquad (66a)$$

Equation (66a) can be validated by developing a second expression for Equation (68), for $\alpha = 2.0$, from the data plotted in Figure 27; namely

$$(\delta_4')_{\bar{\alpha}} = 1.37 \qquad (68b)$$

From Figure 27, for $\alpha = 2.0$,

$$C' = \frac{1}{F(\bar{\alpha},\bar{n})} = \frac{1}{1.36} \qquad (69b)$$

Substituting Equations (67a), (68b), and (69b) into Equation (66) yields

$$\delta_4' = (0.65 + 0.35\alpha)\ \frac{1.37}{1.36}$$

$$\simeq 0.65 + 0.35\alpha \qquad (66b)$$

which is identical to Equation (66a), and thus validates Equation (66a).

Equation (66a) can be used to predict z temperature differences for models that have correctly distorted slopes for a given α; namely $\beta = \alpha$.

The prediction factors for maximum temperature difference data are:

(no depth distortion but possible slope distortion)

$$\delta_1' = \beta \tag{53c}$$

(proper slope distortion for a given α)

$$\delta_2' = 0.70 + 0.30\alpha \tag{57a}$$

The prediction factors for average z temperature difference data are:

(no depth distortion but possible slope distortion)

$$\delta_3' = \beta \tag{62b}$$

(proper slope distortion for a given α)

$$\delta_4' = 0.65 + 0.35\alpha \tag{66a}$$

None of the prediction factors indicate a length scale dependency.

Assuming that the effects of length scale can be neglected the unadjusted data has been analyzed to determine if a valid relation exists between δ and other distortion factors. The distortion factors need to be independent. The depth and the channel roughness were both distorted, and α and β can be considered independent since the channel roughness distortion determines the slope at which the model can operate.

Since the friction factor given by Equation (46) is a function of the channel bottom slope, it can also be considered to be a function of roughness. Thus if the friction factor ratio is defined as

$$\gamma = \frac{f_m}{f}$$

it can also be considered independent of α. Even though the friction factor has not been included as a Pi term, it will still be used in the analysis.

Experimental temperature difference prediction factors for any combination α and β for unadjusted data are defined as

$$\delta_5(x = 2.5) = \delta_5' = \frac{\text{maximum temperature difference, prototype}}{\text{maximum temperature difference, model}}$$

$$\delta_6(x = 2.5) = \delta_6' = \frac{\text{average z temperature difference, prototype}}{\text{average z temperature difference, model}}$$

The prediction factors, δ_5' and δ_6' are listed in Table XII.

The procedure presented by Murphy [12] has been used for determining functions from component equations plotted on logarithmic coordinates. It has been assumed that

$$\delta = f(\alpha,\beta) \tag{70}$$

The component equations are

$$(\delta)_{\bar{\alpha}} = A\beta^p \tag{71}$$

$$(\delta)_{\bar{\beta}} = C\alpha^q \tag{72}$$

Table XII. Prediction factors, length scale and distortion factors

Combination Prototype / Model	n	α	β	γ	Experimental prediction factors δ'_6	Experimental prediction factors δ'_5
C8D3.0 / C4D1.5	2	1.0	1.33	1.35	1.39	1.36
C8D3.0 / C4D2.25	2	1.5	1.33	1.18	1.11	0.98
C8D3.0 / C4D3.0	2	2.0	1.33	1.07	0.96	0.90
C4D1.5 / C2D0.75	2	1.0	0.75	0.74	0.73	0.80
C4D1.5 / C2D1.13	2	1.5	0.75	0.66	0.64	0.62
C4D1.5 / C2D1.5	2	2.0	1.00	0.80	0.65	0.60
C4D2.25 / C2D1.13	2	1.0	0.75	0.76	0.80	0.86
C4D3.0 / C2D1.5	2	1.0	1.00	1.00	0.95	0.91
C8D3.0 / C2D0.75	4	1.0	1.00	1.00	1.01	1.09
C8D3.0 / C2D1.13	4	1.5	1.00	0.89	0.89	0.84
C8D3.0 / C2D1.5	4	2.0	1.33	1.07	0.91	0.82

and a constant is defined as

$$C = \frac{1}{\delta_{\bar{\alpha}|\bar{\beta}}} \tag{73}$$

Equation (50) can be formed by multiplication of the component equations and the constant.

$$\delta = \frac{A\beta^p C\alpha^q}{(\delta)_{\bar{\alpha}|\bar{\beta}}} \tag{70a}$$

To validate Equation (50a) a second component equation for Equation (51) is needed; namely,

$$(\delta)_{\underline{=}} = D\beta^p \tag{72a}$$

If

$$\frac{A\beta^p}{A\beta^p|_{\bar{\beta}}} = \frac{D\beta^p}{D\beta^p|_{\bar{\beta}}} \tag{74}$$

then Equation (50a) is valid.

It has been assumed that

$$(\delta_6') = \frac{A\beta^p C\alpha^q}{(\delta_6')_{\bar{\alpha}|\bar{\beta}}} \tag{70b}$$

The component equations, which are plotted in Figure 28 are

$$(\delta_6')_{\bar{\alpha}} = \beta \tag{71a}$$

$$(\delta_6')_{\underline{=}} = 0.85\beta \tag{71b}$$

and

$$(\delta_6')_{\bar{\beta}} = 1.36\alpha^{-0.53} \tag{72b}$$

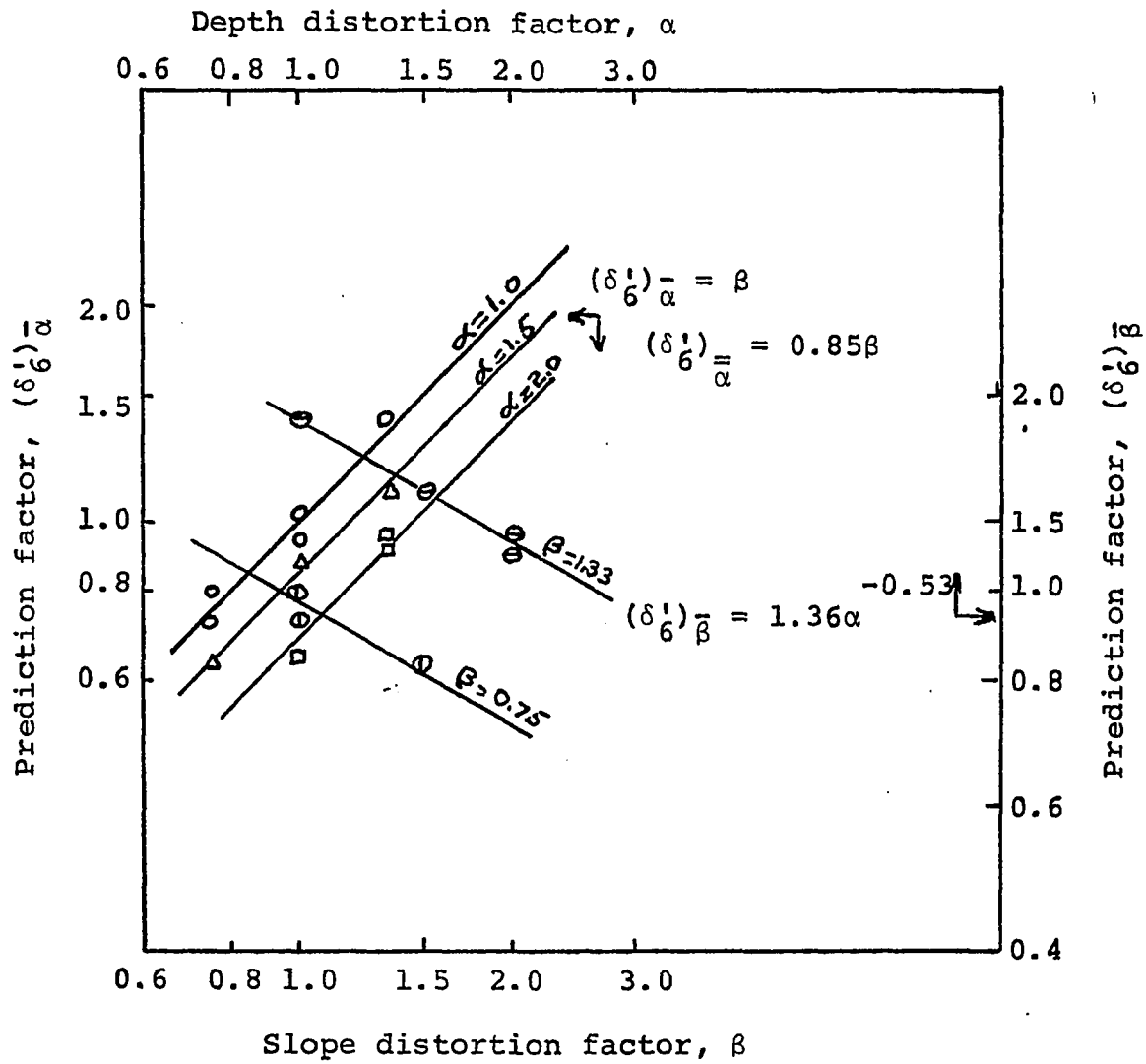

Figure 28. Component equations for the function, δ_6'

where $\bar{\alpha} = 1$, $\bar{\bar{\alpha}} = 1.5$ and $\bar{\beta} = 1.33$.

Substituting Equations (71a) and (71b) into Equation (74) gives

$$\frac{\beta}{\beta\big|_{\beta=1}} = \frac{0.85\beta}{0.85\beta\big|_{\beta=1}}$$

$$\beta = \beta$$

and thus Equation (71a) and (72b) can be combined as a product.

Substituting Equations (71a) and (72b) into Equation (70b) yields

$$\delta_6' = \frac{1.36\alpha^{-0.53}\beta}{1.33}$$

$$= 1.02\beta\alpha^{-0.53} \qquad (70c)$$

The same procedure can be used to develop an expression for δ_5'. It will be assumed that

$$\delta_5' = \frac{A\beta^p C\alpha^q}{(\delta_5')_{\bar{\alpha}|\bar{\beta}}} \qquad (70d)$$

The component equations, which are plotted in Figure 29

$$(\delta_5')_{\bar{\alpha}} = 1.05\beta \qquad (71c)$$

$$(\delta_5')_{\bar{\bar{\alpha}}} = 0.80\beta \qquad (71d)$$

$$(\delta_5')_{\bar{\beta}} = 1.35\alpha^{-0.67} \qquad (72c$$

where $\bar{\alpha} = 1$, $\bar{\bar{\alpha}} = 2$ and $\bar{\beta} = 1.33$.

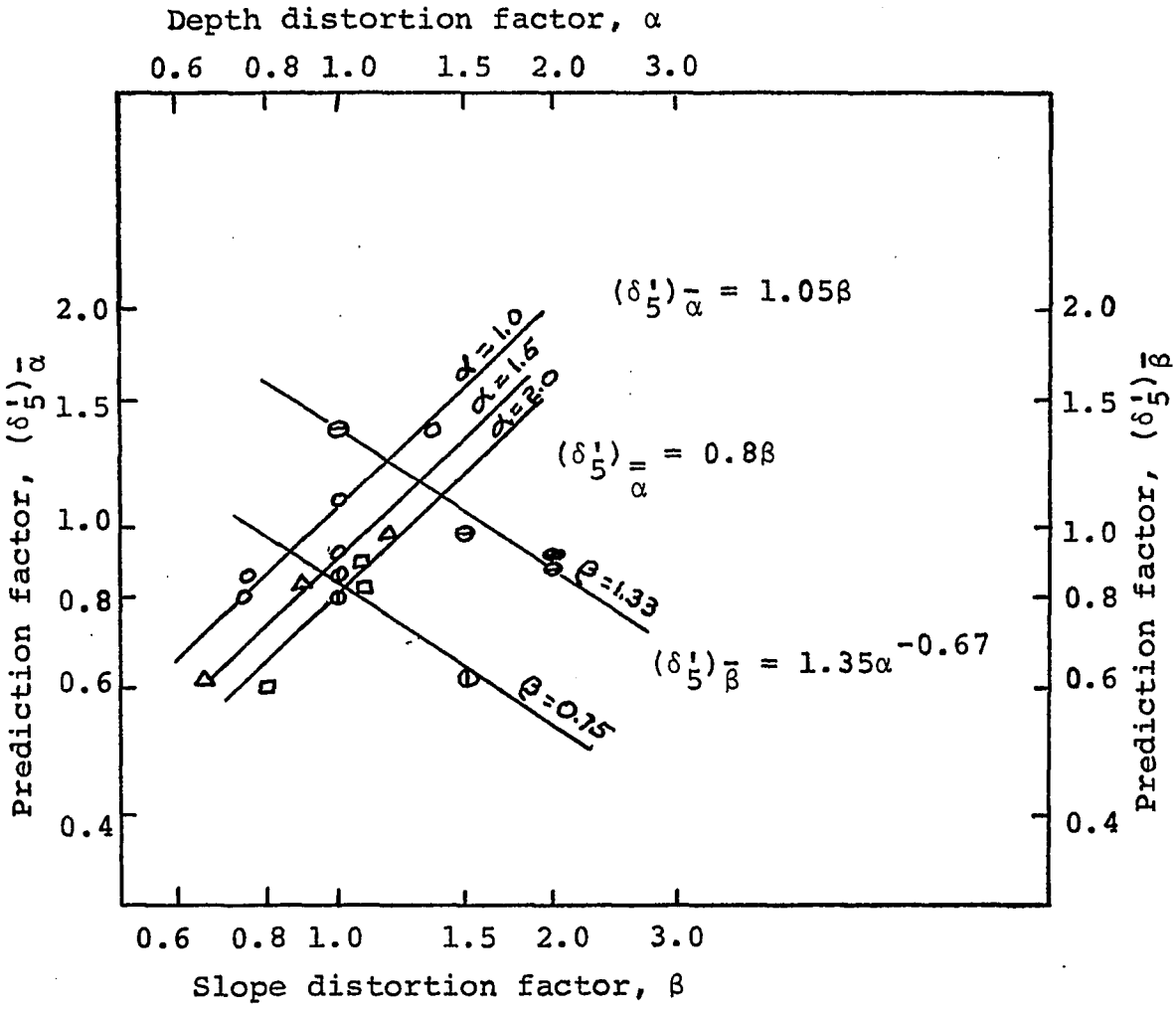

Figure 29. Component equations for the function δ_5'

Substituting Equations (71c) and (71d) into Equation (74) gives

$$\frac{1.05\beta}{1.05\beta}\Big|_{\beta=1} = \frac{0.80\beta}{0.80\beta}\Big|_{\beta=1}$$

$$\beta = \beta$$

and thus Equations (71c) and (71d) can be combined as a product.

Substituting Equations (71a) and (72b) into Equation (70b) yields

$$\delta_5' = \frac{1.35\alpha^{-0.67}\beta}{1.35}$$

$$= \beta\alpha^{0.67} \qquad (70e)$$

The maximum temperature difference prediction factor for models with depth distortion are

$$\delta_2' = 0.70 + 0.30\alpha \qquad (57a)$$

and

$$\delta_5' = \beta\alpha^{-0.67} \qquad (70e)$$

The average z temperature difference prediction factors for models with depth distortion are

$$\delta_4' = 0.65 + 0.35\alpha \qquad (66a)$$

and

$$\delta_6' = 1.02\beta\alpha^{-0.53} \qquad (70c)$$

If in Equations (70e) and (70c), it is assumed that increasing model roughness to achieve $\beta = \alpha$ does not invalidate them, the above four prediction factors result in the

prediction factors listed in Table XIII.

Table XIII. Comparison of prediction factors

Prediction factors for $\beta = \alpha$		Prediction factors Depth distortion factor, α	
		1.5	2.0
Maximum temperature difference			
$\delta_2' = 0.70 + 0.30\alpha$	(57a)	1.15	1.30
$\delta_5' = \beta\alpha^{-0.67} = \alpha^{0.33}$	(70e)	1.14	1.26
Average z temperature difference			
$\delta_4' = 0.65 + 0.35\alpha$	(66a)	1.18	1.35
$\delta_6' = 1.02\beta\alpha^{-0.53} = 1.02\alpha^{0.47}$	(70c)	1.23	1.41

The values in Table XIII show close agreement. For the channel shapes, channel surface conditions, initial temperature differences and the assumptions of the effects of increasing surface roughness, the equations indicate a strong influence of depth distortion on the magnitude of the prediction factor.

If the characteristic length in the Froude Number had been the hydraulic radius, the Froude Number design condition would have been

$$\frac{V_m^2}{gR_m} = \eta \frac{V^2}{gR} \tag{75}$$

For the channels used in this study, and for either n = 2 or n = 4, $\eta = 1.17$ for $\alpha = 1.5$; and $\eta = 1.32$ for $\alpha = 2.0$. The value of η is of the same magnitude as the prediction factors in Table XIII. Removing the distortion in Equation (75) would have to be done by reducing the model velocity, and this should reduce dispersion and reduce δ.

Defining the Froude Number by Equation (75) may be appropriate for prototype-model combinations where the hydraulic radius ratio, R/R_m, departs from n/α. For channels with $\alpha = 1$, R = K (depth) and Equation (75) would not alter the usual velocity ratio.

The downstream limit of the equations in Table XIII may occur somewhat before the temperature difference gradient in the z direction becomes negligible. As this gradient approaches zero, lateral dispersion may no longer cause temperature difference reductions; and dispersion in the vertical direction is minimized because of stratification.

If it is assumed that $\delta_6''(x = 2.5) = \delta_6'' = f(\gamma,\alpha)$ a prediction factor can be developed if two assumptions are made. First, since the data in Table XII show just one value of α for $\bar{\gamma}$, a second point must be assumed. This second point can be established at $\alpha = 1$; and from Equation (53c), $\delta_6'' = \bar{\gamma}$. Second, since only two points are available for determining $(\delta_6'')_{\bar{\gamma}}$, it must be assumed that a straight line between the points adequately expresses the function.

Some support in defining $(\delta_6'')_{\bar{\gamma}}$ can be given by applying the above two assumptions to a new value $\bar{\bar{\gamma}}$. From Figure 30 the equation

$$(\delta_6'') = 1.01\gamma_\alpha^{-0.24}$$

can be formed by multiplication from the two component equations plotted in logarithmic space. Since one set of component equations plot as parallel lines, combination by multiplication is valid. If f were included as a pi term in place of the relative roughness r, then roughness distortion would be apparent in friction factor distortion. The friction factor also depends on α.

C. Prediction Factors for Subsurface Temperatures

Temperatures were measured at two subsurface levels. The position of level 2 temperatures was 1/3 the flow depth below level 1 and the position of level 3 temperatures was 2/3 the flow depth below level 1. The maximum temperature differences at level 2 for C8D3.0, C4D1.5 and C2D0.75 are shown in Figure 31. The maximum temperature difference of C4D1.5 in Figure 31 is approximately 78% lower at x = 2.5 than the difference for C8D3.0. This was approximately the same as the 75% difference noted for the surface temperature differences of the same channels. At x = 2.5 the temperature difference for C2D0.75 is approximately 50% of that of C8D3.0 compared to being

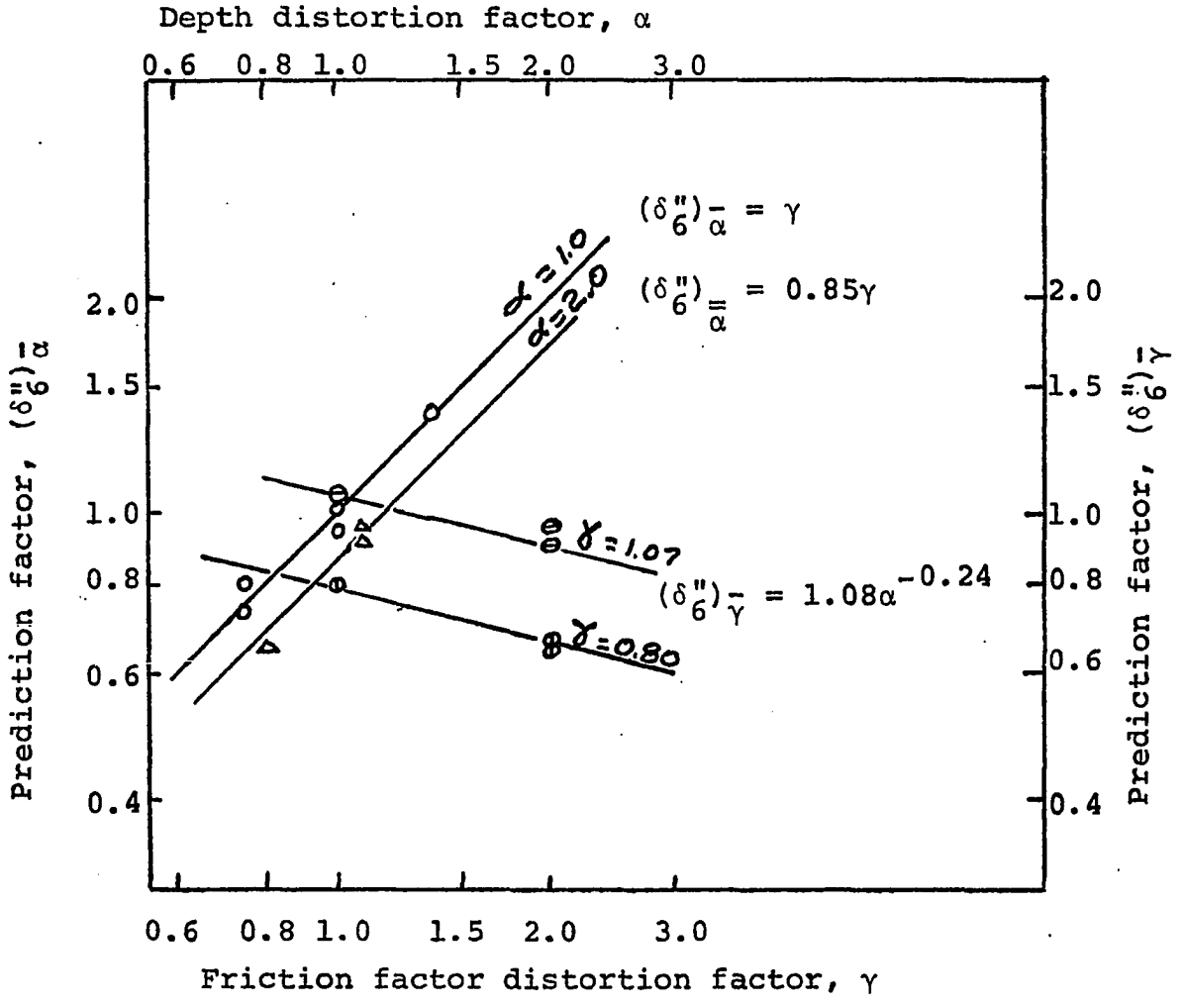

Figure 30. Component equations for the function δ''_6

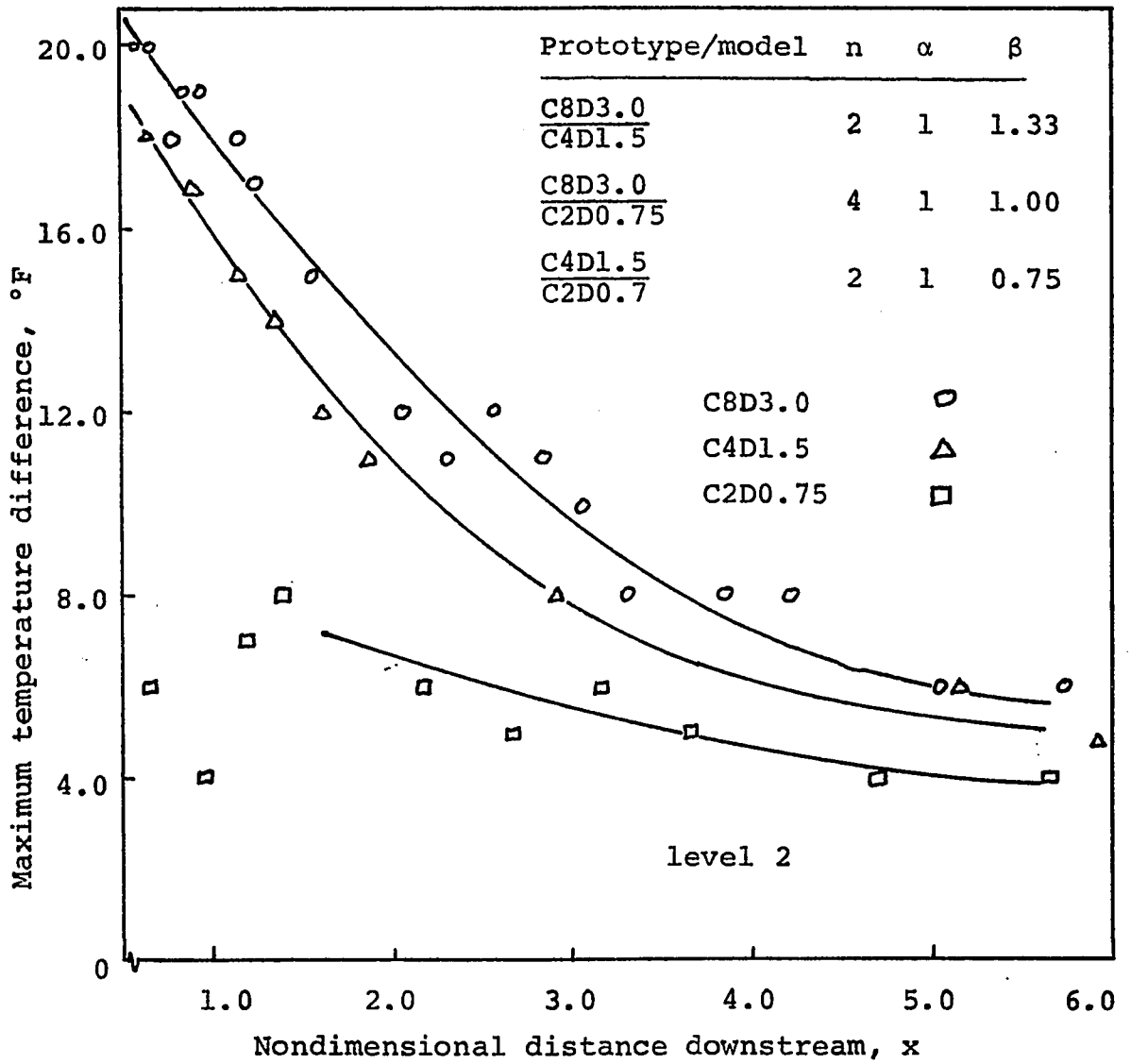

Figure 31. Maximum temperature difference as a function of distance at Level 2 for prototype-model combinations with no depth distortion

approximately 93% of that of C8D3.0 at the surface. The much lower temperatures of C2D0.75 on the second level may have been due to the thermistors in C2D0.75 being at a relatively lower position than those of C8D3.0. The lower position probably resulted because the thermistors for each model had to be placed 2/64 to 3/64 of an inch below the water surface. The probe fixture was always lowered 1/3 the depth, and this probably resulted in the thermistors being 10-15% lower, relatively, in C2D0.75 than in C8D3.0. Since the temperature changed rapidly with vertical distance changes, a small error in position could have resulted in a large temperature difference error.

Another source of error may have been the relatively wide spacing of the thermistors during subsurface level measurements in Channels 2. The spacing was selected to minimize the increase in the combined stream depth due to the flow resistance offered by the steel rods on which the thermistors were mounted. The spacing may have been so wide that a higher temperature between probes may have been missed.

The subsurface maximum temperature difference prediction factors have been listed along with surface prediction factors in Table XIV. For the prototype-model combination of C8D3.0 and C4D1.5 listed in row 1 of Table XIV, where $\alpha = 1$, the

Table XIV. Comparison of prediction factors

Row	Combination $\left(\frac{\text{Prototype}}{\text{Model}}\right)$	n	α	Maximum temperature difference prediction factors at x = 2.5			
				Prediction factor, δ_5' (Equation (70e))	Experimental		
					Level 1	Level 2	Level 3
1	$\frac{C8D3.0}{C4D1.5}$	2	1.0	1.33	1.36	1.25	1.04
2	$\frac{C8D3.0}{C4D2.25}$	2	1.5	1.01	0.98	1.09	1.60
3	$\frac{C8D3.0}{C4D2.25}$	2	2.0	0.84	0.90	1.12	1.60
4	$\frac{C8D3.0}{C2D0.75}$	4	1.0	1.00	1.09	2.00	4.80
5	$\frac{C8D3.0}{C2D1.13}$	4	1.5	0.76	0.84	1.24	3.40
6	$\frac{C8D3.0}{C2D1.5}$	4	2.0	0.84	0.82	1.27	2.00

[a]β = 1.33 for the combinations in rows 1, 2, 3 and 6.
β = 1.00 for the combinations in rows 4 and 5.

experimental prediction factors for levels 1 and 2 are similar enough to lend support to the conclusion reached from surface data that for no depth distortion, heated effluent dispersion in the model, would be the same as the prototype.

The data for combinations with $\alpha > 1$ is shown in Figure 32. For the combination C8D3.0 and C4D3.0 listed in row 3 of Table XIV, where $\alpha = 2$, the prediction factor is larger for level 2 than for level 1 even considering the possible scatter in the data.

When $\delta < 1$ at level 1 a higher temperature exists in the model than in the prototype. If the temperature were higher at the model surface it would indicate less dispersion than in the prototype, and therefore the temperatures at the subsurface levels in the model would be expected to be lower than those of the subsurface positions of the prototype. This would lead to $\delta_{surface} < \delta_{subsurface}$ as is indicated in row 3 of Table XIV.

The data for level 3 which is shown in Figure 33 and 34 and listed in Table XIV does not entirely support the conclusion of similar dispersion for $\alpha = 1$, and $\delta_{surface} < \delta_{subsurface}$. However at this level the temperature differences did not exceed 5°F and the accuracy of the data may be strongly influenced by errors of 0.5 to 1.0°F in the temperature observations.

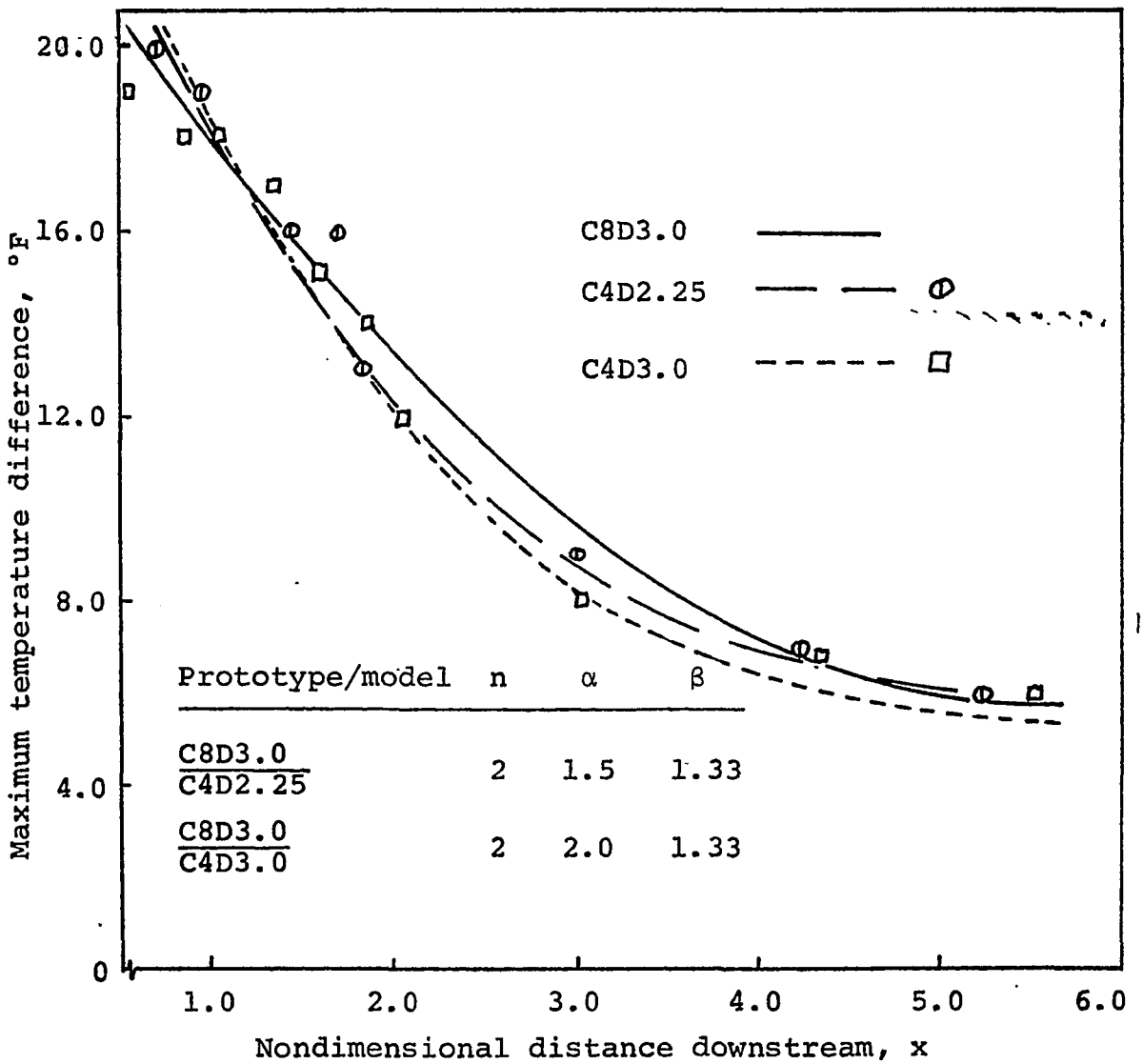

Figure 32. Maximum temperature difference as a function of distance at Level 2 for prototype-model combinations with depth distortion

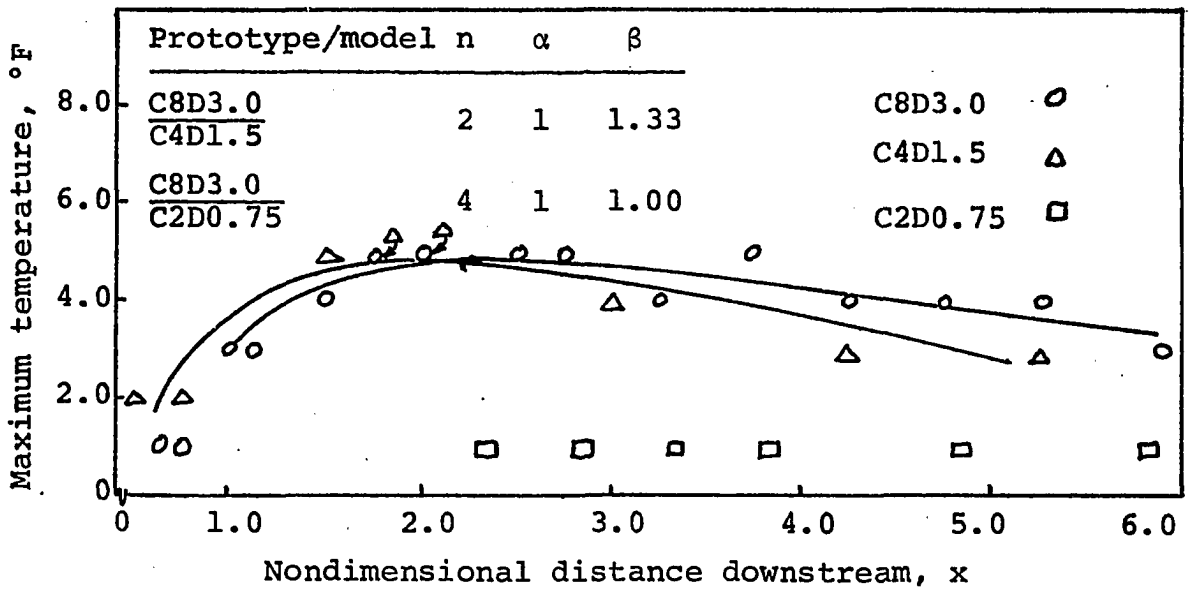

Figure 33. Maximum temperature difference as a function of distance at Level 3 for prototype-model combinations with no depth distortion

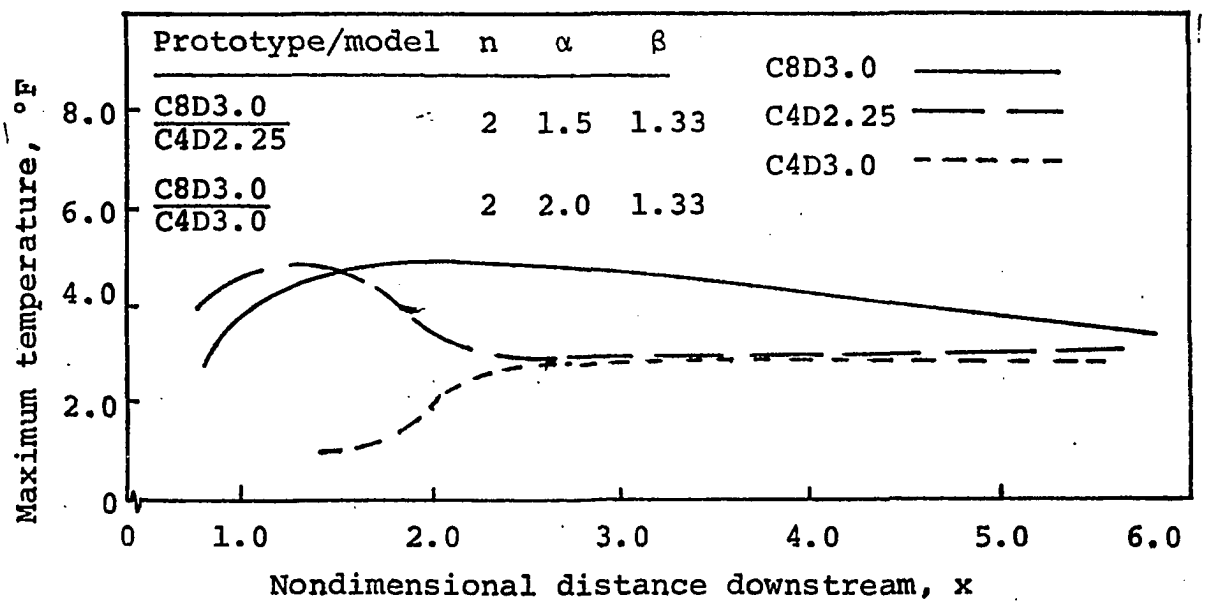

Figure 34. Maximum temperature difference as a function of distance at Level 3 for prototype-model combinations with depth distortion

VII. SUMMARY AND CONCLUSIONS

Engineering similitude was used to design models for predicting temperature patterns in open channel flow. Some design conditions were distorted. Distortion resulted from the choice of model fluid, model surface conditions and from intentional distortion of such vertical dimensions as the model flow depth.

Seven channel systems were experimentally studied. Each system consisted of a main channel of trapezoidal cross section conveying water at 60°F and an intersecting smaller channel of rectangular cross-section which discharged heated water at 80°F into the main channel. Pairs of the seven channel systems provided various prototype-model combinations with different combinations of design condition distortions. Temperatures at the surface and two subsurface layers were measured. Prediction factors for surface temperature differences were developed for models with slope distortion, vertical dimension distortion and a combination of slope and depth distortion.

It was estimated that for models with depths twice the magnitude of that required by the horizontal length scale, the surface temperatures would be approximately three-fourths the magnitude of those in the prototype at a distance of 2.5 channel widths downstream from the introduction of the heated effluent.

The study revealed that depth distortion in the models produced a significant distortion of the temperatures at the water surface of the model. Subsurface temperatures appear to be distorted opposite to surface temperatures.

VIII. SUGGESTIONS FOR FUTURE STUDY

The main stream reservoir and the heated effluent reservoir should have continuous makeup flow to minimize variations in flow rates during a run and to facilitate longer duration runs. Flow rate capability in excess of that used in this study would be desirable to enable the smaller model to be operated out of the laminar-turbulent transition region.

A means of obtaining instrument averaged temperature readings would be desirable.

Depth distortion should be studied in channels where sufficient roughness has been added to allow the models to be operated at the slopes dictated by design conditions.

An experimental program involving channels used in this study and wide channels would be desirable to determine the influence of hydraulic radius distortion.

IX. LITERATURE CITED

1. D.I.H. BARR, The Engineer, 215, 345 (1963).

2. D.I.H. BARR, The Engineer, 216, 885 (1963).

3. D.I.H. BARR, The Engineer, 222, 625 (1966).

4. J. R. BULL, "Simulation of Heated Effluent Dispersion in an Open Channel," Unpublished Ph.D. dissertation, Iowa State University (1970).

5. VEN TE CHOW, Open-Channel Hydraulics, McGraw-Hill Book Inc., New York (1959).

6. J. E. EDINGER and E. M. POLK, "Initial Mixing of Thermal Discharges into a Uniform Current," National Center for Research and Training in the Hydrologic and Hydraulic Aspects of Water Pollution Control, Report Number 1, Vanderbilt University (1969).

7. J. W. ELDER, Journal of Fluid Mechanics, 5, 4 (1959).

8. J. O. HINZE, Turbulence, McGraw-Hill Book Company, Inc., New York, (1959).

9. W. FRAZER, D.I.H. BARR, and A. A. SMITH, "A Hydraulic Model Study of Heat Dissipation at Longannet Power Station," Proceedings, Institution Civil Engineers (1968).

10. A. T. IPPEN (ed.), Estuary and Coastline Hydrodynamics, McGraw-Hill Book Company, Inc., New York (1966).

11. D. MERRIMAN, Scientific American, 222, 42 (1970).

12. G. MURPHY, Similitude in Engineering, The Ronald Press Company, New York, (1950).

13. National Symposium on Thermal Polution, Biological Aspects of Thermal Pollution, P. A. Krenkel and F. L. Parker, Eds., Vanderbilt University Press, Nashville, Tennessee, (1969).

14. F. L. PARKER and P. A. KRENKEL, Physical and Engineering Aspects of Thermal Pollution, Chemical Rubber Company Press (1970).

15. Proceedings of the National Symposium on Thermal Pollution, Engineering Aspects of Thermal Pollution, F. L. Parker and P. A. Krenkel, Eds., Vanderbilt University Press, Nashville, Tennessee (1969).

16. J. ROMM, (ed.), Thermal Pollution: A Short Course, Number 30, Water Resources and Marine Sciences Center, Cornell University (1970).

17. D. J. TUNSTALL, "Thermal Analogy for the Diffusion of Neutrons in a Two Core Reactor", Unpublished M.S. thesis, Iowa State University (1970).

18. J. K. VENNARD, Elementary Fluid Mechanics, 3 ed., John Wiley and Sons, Inc., New York (1954).

X. ACKNOWLEDGMENTS

The author wishes to express his sincere appreciation to Dr. Glenn Murphy for his guidance throughout the development of this dissertation. Gratitude is expressed to the Iowa State University Nuclear Engineering Department for funding the study.

A special note of thanks is due my wife, Marilyn, for her help in data recording and typing the draft of this dissertation.

XI. APPENDIX:

NORMALIZED AND AVERAGED TEMPERATURE DIFFERENCES, °F

Channel C8D3.0 - Level 1

Temperature differences

x	z														
	-0.53	-0.46	-0.40	-0.34	-0.28	-0.21	-0.15	-0.09	0.03	0.04	0.10	0.16	0.23	0.29	0.35	0.41
0.13	2	2	1	0												
0.25	20	13	7	1												
0.38	20	20	16	8	4	1	0									
0.50	20	20	20	15	8	4	1									
0.63	20	20	20	18	13	8	7	1	0							
0.75	18	20	19	19	17	12	6	4	1	0						
0.88	9	15	18	19	18	11	8	4	1	0						
1.00	8	12	15	18	18	14	12	8	3	1	0					
1.13	7	12	12	16	17	18	13	10	4	2	1	0	0			
1.25	9	10	12	14	16	17	13	8	4	2	1	0				
1.38	8	10	11	12	15	16	16	12	4	2	1	0				
1.50	9	11	12	13	13	15	15	14	8	6	2	0				
1.75	8	11	12	13	14	14	13	8	6	4	2	1	0			
2.00	8	11	12	13	13	14	13	13	12	9	7	7	2	2	0	
2.25	8	9	11	11	11	13	13	1	10	10	7	5	2	1	1	0
2.50	8	8	10	11	11	12	12	12	11	9	9	7	6	3	1	0
2.75	8	9	10	11	11	12	12	12	11	10	9	7	4	3	1	1
3.38	7	7	7	8	10	10	10	11	10	10	8	6	6	3	1	1
3.75	6	6	6	6	8	9	9	9	8	9	8	8	7	6	3	2
5.00	6	5	6	7	7	7	7	8	8	8	8	8	8	7	5	4
5.63	5	4	5	5	5	5	6	6	7	7	7	7	7	7	7	5
6.25	4	4	4	4	5	5	6	5	6	6	7	7	6	6	6	5

Channel C8D3.0 - Level 2

	Temperature differences							
	z							
x	-0.50	-0.38	-0.25	-0.13	0.0	0.13	0.25	0.38
0.25	6	0						
0.38	17	0						
0.50	20	6	0					
0.63	20	13	2	0				
0.75	18	17	3	0				
0.88	18	19	7	1	0			
1.0	17	19	9	1	0			
1.13	17	18	10	2	0			
1.25	16	17	11	2	0			
1.50	14	15	12	5	1	0		
1.75	11	14	12	8	1			
2.00	7	12	12	8	3	0		
2.25	6	11	11	9	8	1	0	
2.50	6	8	12	10	3	1	0	
2.75	5	7	11	10	5	1	0	
3.0	4	7	10	9	6	2		
3.25	4	6	8	8	6	2	0	0
3.75	3	4	8	8	7	4	1	0
4.13	3	3	7	8	7	5	2	0
5.00	3	4	5	6	6	6	4	1
5.63	3	3	4	6	6	6	4	3
6.25	3	3	4	5	5	4	2	1

Channel C8D3.0 - Level 3

Temperature differences

x	z = -0.50	-0.38	-0.25	-0.13	0.0	0.13	0.25	0.38
0.13	0							
0.25	0							
0.38	1	0						
0.50	1	0						
0.75	3	1	0					
0.88	3	2	1	0				
1.00	2	4	2					
1.25	2	4	2					
1.50	1	5	4	0				
1.75	2	5	4	1				
2.00	2	4	5	2	0			
2.25	1	5	4	4	1	0		
2.50	1	3	5	3	1	0		
3.00	1	2	4	4	2	1		
3.50	1	2	5	4	2	1	0	
4.00	1	2	3	4	2	1	1	0
4.50	1	2	4	4	2	1	0	
5.00	1	1	3	4	3	2	1	0
5.63	1	1	2	3	3	2	1	1
6.25	1	1	2	2	3	2	1	0

Channel C4D1.5 - Level 1

Temperature differences

	z											
x	-0.59	-0.50	-0.47	-0.38	-0.28	-0.19	-0.09	0.0	0.9	0.19	0.28	0.38
0.08	20	7	5	1	0	0						
0.20	20	18	17	4	2	0	0	0				
0.32	20	20	20	13	25	1	0	0				
0.45	20	20	20	19	10	2	0	0				
0.58	20	20	20	20	35	3	1	0				
0.70	13	19	20	20	16	9	1	0				
0.82	4	6	8	20	19	12	4	1	0	0		
0.95	3	5	7	10	19	16	5	2	0	0		
1.08	3	5	6	9	16	17	7	2	1	0		
1.33	4	4	5	8	11	14	11	5	1	1	0	
1.58	4	4	6	8	11	12	11	6	2	1	1	0
1.83	5	4	5	8	9	11	11	9	5	1	1	1
2.82	4	4	5	6	7	8	8	8	5	4	3	2
4.07	5	5	5	6	6	7	7	7	6	4	4	2
5.07	5	5	5	5	6	6	6	6	5	4	3	2
6.07	5	5	4	5	5	5	5	6	5	5	4	3

Channel C4D1.5 - Level 2

Temperature differences

x	z = -0.50	-0.38	-0.19	0.0	0.19	0.38
0.08	0					
0.32	17	5	0			
0.58	12	18	5	0		
0.82	7	18	7	0		
1.08	6	15	13	0		
1.33	3	14	12	1		
1.58	2	12	12	3	0	
1.83	2	11	11	4		
2.82	3	6	8	6	3	0
4.07	3	5	7	6	4	1
5.08	3	4	5	6	5	2
6.07	4	3	4	5	5	3

Channel C4D1.5 - Level 3

x	z = -0.50	-0.38	-0.19	0.0	0.19	0.38
0.08	0	0				
0.32	2	0				
0.58	2	1	0			
0.82	1	2	0			
1.08	2	4	2	0		
1.33	1	5	4	0		
1.58	1	4	5	0		
1.83	1	5	4	1		
2.82	1	3	4	2		
4.07	3	2	3	3	1	
5.08	2	2	3	3	2	0
6.07	3	2	3	3	3	2

Channel C4D2.25 - Level 1

Temperature differences

	z											
x	-0.59	-0.50	-0.47	-0.38	-0.28	-0.19	-0.09	0.0	0.09	0.19	0.28	0.38
0.15	17	1	3	0								
0.28	11	16	16	2	1							
0.40	20	16	14	4	2	1	0	0				
0.53	20	20	19	9	2							
0.65	20	20	20	14	5	2	1					
0.78	16	20	20	19	9	4						
0.90	16	17	19	20	12	5	2	1				
1.03	15	17	18	19	13	6	2	2				
1.15	13	16	17	19	14	5	3	1	1			
1.40	14	16	17	18	14	8	3	1	1			
1.65	12	15	16	17	13	10	4	2	1			
1.90	13	14	15	15	14	10	6	4	1	1	0	
2.90	12	11	11	11	11	10	7	3	2	1	1	1
4.15	10	10	10	10	10	8	8	5	2	1	2	2
5.15	9	8	9	9	8	8	7	7	3	2	2	2
6.15	7	8	8	7	7	6	6	6	5	4	4	3

Channel C4D2.25 - Level 2

Temperature differences

	z											
x	-0.59	-0.50	-0.47	-0.38	-0.28	-0.19	-0.09	0.0	0.9	0.19	0.28	0.38
0.40	20	15	8	0								
0.65	20	20	19	6	1							
0.90	11	17	19	16	6	0						
1.15	12	16	17	16	9	2	0					
1.40	10	16	16	15	6	3	0	0				
1.65	9	14	16	14	9	4	1	0				
1.90	8	14	13	13	8	3	0					
2.90	8	8	9	8	7	3	1	1				
4.15	6	7	7	7	7	5	3	2				
5.15	6	6	6	6	6	4	3	1	1			
6.15	5	6	5	5	5	5	3	3	1	1		

Channel C4D2.25 - Level 3

	Temperature differences					
	z					
x	-0.50	-0.38	-0.19	0.0	0.19	0.38
0.15	0	0				
0.40	1	0				
0.65	4	0				
0.90	5	1	0			
1.15	5	3	0			
1.40	5	3	0			
1.65	4	2	0			
1.90	3	3	0			
2.90	3	2	1	0		
4.15	3	3	1	0		
5.15	3	2	1	0		
6.15	3	2	1	0		

Channel C4D3.0 - Level 1

Temperature differences

	z											
x	-0.59	-0.50	-0.47	-0.38	-0.28	-0.19	-0.09	0.0	0.09	0.19	0.28	0.38
0.13	16	6	7	2	1	0	0					
0.38	20	17	16	9	7	3	1	0	0			
0.63	19	20	20	16	11	7	4	1	0	0		
0.88	13	18	18	19	16	8	6	3	2	0	0	
1.13	12	13	13	18	16	11	10	5	2	1	0	
1.38	11	13	12	17	16	11	9	6	3	1	1	
1.63	11	11	11	14	16	13	8	7	5	2	2	2
1.88	10	11	11	13	14	14	10	7	5	4	3	2
2.88	9	9	10	10	11	10	9	9	7	7	5	4
4.13	7	8	8	9	9	9	8	8	7	6	6	6
5.13	7	7	8	8	9	8	8	7	7	6	6	6
6.13	7	7	7	7	7	8	7	7	6	6	7	6

Channel C4D3.0 - Level 2

Temperature differences

	z										
x	-0.59	-0.50	-0.47	-0.38	-0.28	-0.19	-0.09	0.0	0.9	0.19	0.28	0.38
0.15	3											
0.40	19	10	7	0	0							
0.65	18	18	17	8	1	0	0					
0.90	13	18	19	14	8	1	0	0				
1.15	13	16	17	17	12	4						
1.40	10	15	15	15	11	7	0					
1.65	8	13	14	13	9	7	1	1				
1.90	7	11	11	12	11	8	3	1	0			
2.90	5	8	8	8	8	7	6	1	0			
4.15	5	6	6	7	6	6	4	1	1	1	1	
5.15	4	5	5	5	6	5	4	4	3	2	1	
6.15	4	3	5	5	5	5	5	5	3	2	1	1

Channel C4D3.0 - Level 3

Temperature differences						
	z					
x	-0.50	-0.38	-0.19	0.0	0.19	0.38
0.88	1	0				
1.13	1	1	0			
1.38	1	1	0			
1.63	1	2	1	0		
1.88	1	2	1	0		
2.88	3	2	2	0		
4.13	3	3	2	1	0	
5.13	2	3	3	1	0	
6.13	3	3	2	1	1	1

Channel C2D0.75 - Level 1

Temperature differences										
	z									
x	-0.56	-0.44	-0.31	-0.19	-0.06	0.06	0.19	0.31	0.44	0.56
0.10	20	4	1	0						
0.35	20	20	13	1	1	0				
0.60	20	20	20	9	6	1	1	0		
0.85	9	16	20	14	9	2	1	0		
1.10	8	10	15	18	11	8	1	0		
1.35	5	9	14	14	12	9	1	0		
1.60	4	7	12	13	11	9	4	1	0	
2.10	2	5	12	12	11	11	8	6	2	2
2.60	3	3	8	11	10	9	8	6	5	2
3.10	2	2	5	9	10	9	9	8	7	1
3.60	2	2	3	7	8	8	9	8	7	3
4.60	3	2	4	5	7	8	8	8	6	4
5.60	3	3	3	5	6	7	6	7	6	4

Channel C2D0.75 - Level 2

Temperature differences

x	z = -0.56	-0.28	0.0	0.28	0.56
0.10	0	0			
0.35	2	0			
0.60	6	0			
0.85	3	4	0		
1.10	1	7	0		
1.35	1	8	1	0	
1.60	1	8	2	0	
2.10	1	6	4	0	
2.60	1	4	5	1	0
3.10	1	4	6	3	1
3.60	1	3	5	3	1
4.60	0	1	4	3	2
5.60	1	1	4	4	3

Channel C2D0.75 - Level 3

Temperature differences

x	z = -0.56	-0.28	0.0	0.28	0.56
0.10	0				
0.35	0				
0.60	0				
1.10	0				
1.60	0				
2.10	0	1			
2.60	0	1			
3.10	0	1			
3.60	0	1			
4.60	0	1	1	1	1
5.60	0	1	1	1	0

Channel C2D1.13 - Level 1

Channel C2D1.13 - Level 2

Temperature differences

	z							z						
x	-0.63	-0.38	-0.13	0.13	0.38	0.63	x	-0.63	-0.38	-0.13	0.13	0.38	0.63
0.22	20	1	0				0.22	2	0				
0.48	20	6	1	0			0.48	9	0				
0.73	20	20	3	0			0.73	15	2				
0.98	17	20	6	0			0.98	12	10				
1.22	11	20	7	1	0		1.22	12	15	0			
1.48	7	19	7	3	0		1.48	12	14	0			
1.73	6	16	12	4	0		1.73	8	13	0			
1.98	6	16	12	5	1	0	2.22	5	10	1	0		
2.22	4	16	12	6	1	0	2.73	4	8	2	0		
2.73	5	14	11	5	2	1	3.22	4	7	3	1	0	
3.22	7	13	10	5	2	1	3.73	3	6	4	1	1	
3.73	5	12	10	4	3	1	4.73	4	5	4	3	2	1
4.73	6	8	8	7	5	2	5.73	4	4	4	2	2	2
5.73	6	6	7	7	4	4							

Channel C2D1.13 - Level 3

	Temperature difference				
	z				
x	-0.63	-0.38	-0.13	0.13	0.38
0.22	0	0			
0.48	0	0			
0.73	0	0			
1.22	0	0	0		
1.73	1	1	0		
2.22	1	2	0		
2.73	1	1	0		
3.22	0	1			
3.73	0	0	0		
4.73	1	1			
5.73	1	1	1	1	

Channel C2D1.5 - Level 1

	Temperature difference					
	z					
x	-0.67	-0.38	-0.13	0.13	0.38	0.67
0.20	19	6	1	0		
0.45	22	12	3	1	0	
0.70	20	19	3	2	0	
0.95	18	20	6	2	0	
1.20	15	20	7	3	0	
1.45	13	19	9	4	0	
1.70	12	18	9	4	1	0
1.95	12	17	11	4	1	0
2.20	11	17	10	4	1	0
2.70	10	14	10	5	2	0
3.20	9	13	10	6	2	1
3.70	9	11	9	7	2	1
4.70	8	9	9	7	2	2
5.70	7	8	8	6	2	2

Channel C2D1.5 - Level 2

Temperature differences

x	z = -0.67	-0.38	-0.13	0.13	0.38	0.67
0.20	1					
0.45	7					
0.70	8	0				
0.95	16	1	0			
1.20	12	6				
1.45	11	10	0			
1.70	8	10	0			
2.20	6	9	1			
2.70	5	9	1			
3.20	5	9	2			
3.70	4	7	3			
4.70	4	6	3	1		
5.70	4	6	4	1		

Channel C2D1.5 - Level 3

x	z = -0.65	-0.33	0.0	0.33	0.65
0.20	0				
0.45	1				
0.70	0	0			
0.95	3	1			
1.20	3	1			
1.70	2	1			
2.20	2	1	1		
2.70	2	2	1		
3.70	2	2	1	1	
4.70	2	3	1	1	
5.70	2	3	2	1	